


ORIGINAL PAPER

Open Access



# Impact of mechanical stratigraphy on deformation style and distribution of seismicity in the central External Dinarides: a 2D forward kinematic modelling study

Philipp Balling<sup>1\*</sup> , Bruno Tomljenović<sup>2</sup>, Marijan Herak<sup>3</sup> and Kamil Ustaszewski<sup>1</sup>

## Abstract

The External Dinarides fold-thrust belt formed during Mid-Eocene–Oligocene times by SW-propagating thrusting from the Internal Dinarides towards the Adriatic foreland. Although previously considered as structurally quite uniform, recent work reported along-strike contrasting deformation styles in two structural domains within this fold-thrust belt. The two areas with very contrasting deformation styles are separated by the N–S-striking dextral Split-Karlovac Fault, a 250 km long, transpressive transfer fault. The southeastern domain is characterized by a thin-skinned SW-vergent nappe stack in contrast to the northwestern domain, where a set of blind, thick-skinned top-SW thrust duplexes prevail underneath the passive NE-vergent backthrusts. To better understand why the External Dinarides underwent such contrasting along-strike deformation, we reconsidered a temporal and spatial along- and across-strike distribution of Paleo-Mesozoic lithofacies to both sides of the Split-Karlovac Fault and estimated the role of mechanical stratigraphy on deformation styles in this part of the fold-thrust belt. Therefore, we constructed a new 2D kinematic forward model in the western backthrust-dominated domain. Our best-fit forward-modelled balanced cross section across the central Velebit Mtn. portrays a 75 km wide triangle zone. This zone took up at least 47 km of shortening during Eo–Oligocene times. It comprises a set of thin-skinned NE-vergent backthrusts detached in the upper Paleozoic atop a SW-vergent thick-skinned antiformal stack detached in the lower Paleozoic Adriatic basement. The NE-vergent backthrusts likely nucleated at lateral facies boundaries related to extensional half grabens that locally formed during Middle Triassic and Late Jurassic passive margin extension. During the Eo–Oligocene folding and thrusting, the selective inversion of inherited Mesozoic half grabens boundary faults into the NE-vergent backthrusts in the northwestern domain led to the observed along-strike changes in the deformation style of the External Dinarides. A seismotectonic analysis of instrumentally recorded earthquakes suggests contrasting seismic behaviour along the central and southern Velebit transects within the northwestern structural domain. The central Velebit Mtn. triangle structure appears to currently accommodate dominantly strike-slip motion, with reverse faulting being confined to east of the Split-Karlovac Fault. In contrast, seismicity along the southern Velebit cross section appears to be confined to the structurally lowermost parts of the triangle zone and the foreland, while its structurally higher parts are less seismically active. Also, a predominance of reverse faulting along this transect suggests ongoing accommodation of shortening in this part. Our results indicate that both the variations in the mechanical stratigraphy and the

Editorial handling: Stefan Schmid.

\*Correspondence:

Philipp Balling

philipp.balling@uni-jena.de

Full list of author information is available at the end of the article



© The Author(s) 2023. **Open Access** This article is licensed under a Creative Commons Attribution 4.0 International License, which permits use, sharing, adaptation, distribution and reproduction in any medium or format, as long as you give appropriate credit to the original author(s) and the source, provide a link to the Creative Commons licence, and indicate if changes were made. The images or other third party material in this article are included in the article's Creative Commons licence, unless indicated otherwise in a credit line to the material. If material is not included in the article's Creative Commons licence and your intended use is not permitted by statutory regulation or exceeds the permitted use, you will need to obtain permission directly from the copyright holder. To view a copy of this licence, visit <http://creativecommons.org/licenses/by/4.0/>.

pre-orogenic structural inheritance obtained during rifting and passive margin stages exert control on contractional structures within the External Dinarides, including the distribution of present-day seismicity.

**Keywords** passive roof thrust, triangle zone, duplex, structural inheritance, balanced cross-sections, Seismicity, Velebit Mtn

## 1 Introduction

Mechanical stratigraphy, the concept of assigning mechanical properties to rock successions, facilitates the understanding of factors controlling the style and location of deformation of the Earth's crust (e.g. Rich, 1934; Corbett et al., 1987; Dahlstrom, 1970). This relationship is not only evident from outcrop and borehole data (e.g. Corbett et al., 1987; Narr, 1991; Wilkins & Gross, 2002; Laubach et al., 2009), but also from analogue (e.g. Mulugeta & Koyi, 1992; Turrini et al., 2001; Ravaglia et al., 2004) and numerical models (e.g. Cooke et al., 1999; Dean et al., 2013). They show that heterogeneities in mechanical properties within rock layers lead to the localization of strain in mechanically weak layers. Variation in fracture density, thickness (e.g. McQuillan, 1973; Narr, 1991) and location of mechanically weak and strong layers control the position of the detachment level and ramp-flat geometries of faults. Spatial and temporal three-dimensional lithofacies variations within an undeformed sedimentary succession result in a complex multilayer mechanical stratigraphy (Cawood & Bond, 2018). This can control strain partitioning, which in turn leads to along-strike contrasting styles of deformation within fold and thrust belts (Dean et al., 2013). An even more complex pattern arises if the mechanical stratigraphy is altered by pre-orogenic faults. The development of fundamental mechanical (e.g. Davis et al., 1983; Dahlen, 1990) and geometrical deformation concepts (e.g. Verrall, 1981; Suppe, 1983; Gibbs, 1983; Suppe & Medwedeff, 1990; Withjack & Peterson, 1993), numerical (e.g. Buiter et al., 2009; Erdős et al., 2014; Granado & Ruh, 2019) and analogue models (e.g. Graveleau et al., 2012; Zwaan et al., 2022) have shown that inherited structures also exert control on the style of deformation in orogenic systems. For example, the inversion of pre-existing normal faults during contractional phases is frequently reported in fold-and-thrust belts formed at Mesozoic passive continental margins within the circum-Mediterranean

region, e.g. in the Alps (e.g. Davies, 1982; De Graciansky et al., 1989; Coward et al., 1991; Coward, 1996; Homberg et al., 2002; Butler et al., 2006; Malz et al., 2016), in the Pyrenees (e.g. Hayward & Graham, 1989; Casas-Sainz & Simón-Gómez, 1992; Guimerà et al., 1995; Vergés et al., 2002), and in the Apennines (e.g. Tavarnelli, 1996; Scisciani et al., 2002; Tavarnelli et al., 2004; Butler et al., 2006; Scisciani & Calamita, 2009; Scisciani, 2009).

In the Dinarides fold-thrust belt, a possible impact of pre-existing Mesozoic extensional structures on the present structural architecture was not yet investigated in detail. Situated in the north-central Mediterranean region, the external part of the Dinarides was previously considered as structurally fairly uniform along its entire c. 700 km long strike (Fig. 1a) until Balling et al. (2021b) showed that the central part of the External Dinarides is characterized by substantially contrasting deformational styles observed to both sides of the N–S-striking dextral Split-Karlovac Transfer Fault (Fig. 1c). Based on two regional-scale, balanced and kinematically forward-modeled cross-sections to both sides of the Split-Karlovac Fault (Fig. 1d, e), they showed that the structural domain to the northwest of this fault is characterized by a triangle zone composed of thick-skinned and SW-propagating thrust duplexes, topped by a thin-skinned passive top-NE roof backthrust (Fig. 1d). A minimum crustal shortening along this cross-section was estimated to some 89 km. By contrast, the structural domain to the southeast of the Split-Karlovac Fault is characterized by thin-skinned and in-sequence SW-propagating thrusts along a stepwise shallowing foreland-propagating detachment (Fig. 1e). Minimum crustal shortening along this cross-section is estimated to some 127 km. Based on these cross-sections Balling et al. (2021b) proposed that the N–S striking segment of the Split-Karlovac Fault acted as a dextral transfer fault zone separating the two structural domains with contrasting deformational styles (Fig. 1).

(See figure on next page.)

**Fig. 1** **a** Topographic map of the northern central Mediterranean realm. The Dinarides fold-and-thrust belt is bounded by the Southern Alps in the north and by the Hellenides in the south. **b** The Velebit Mtn. are located within the northern External Dinarides and form a well pronounced up to 1758 m high topographic barrier along the northeastern Adriatic coast. The hinterland of the southern and central Velebit is characterized by the Lika Plateau at the average elevation of 560 m a.s.l. **c** Tectonic map of the Dinarides fold-and-thrust belt (Balling et al., 2021b; Schmid et al., 2020) showing the locations of the study area and the cross-sections presented in **d** and **e** and in Fig. 8. Contrasting deformational styles in two structural domains to the west and east of the Split-Karlovac Fault (SKF) are shown in **d** Southern Velebit cross-section and in **e** Split cross-section, both modified from (Balling et al., 2021b). The major detachments shown in two cross-sections are colour-coded according to their stratigraphic levels

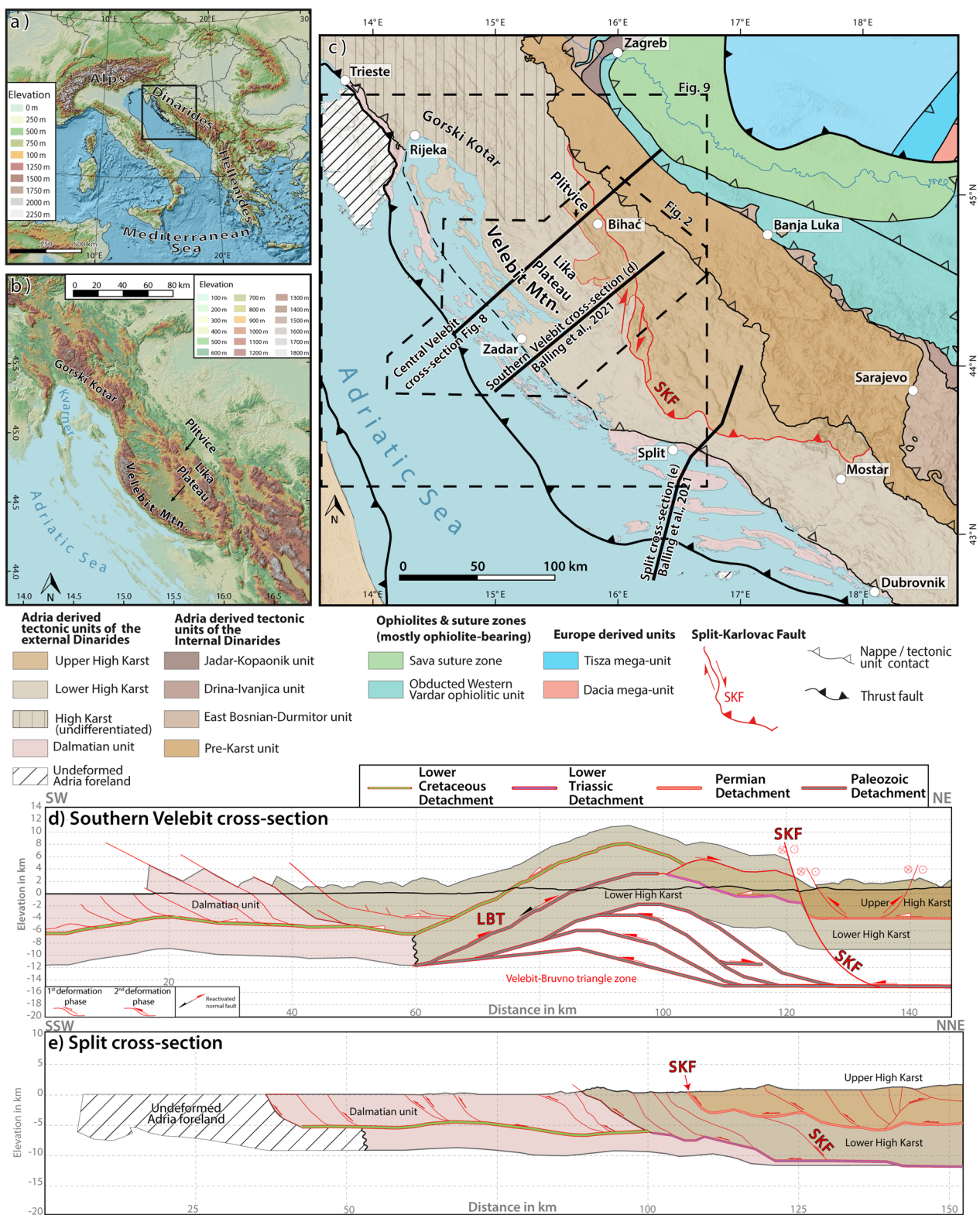


Fig. 1 (See legend on previous page.)



In this paper we extend the study area of Balling et al. (2021b) further to the NW into the central part of the External Dinarides, now also comprising the central part of the Velebit Mtn., the Lika Plateau and the Plitvice area (Fig. 1b, c). This extension served: (i) to explore whether the triangle zone, reported from the southern Velebit Mtn. (Fig. 1d), continues along-strike further NW into the central Velebit Mtn., and, (ii) to review possible differences in the structural architecture within the Velebit Mtn. and neighbouring areas. Furthermore, we evaluated potential factors controlling the formation of the triangle zones to answer the question why the External Dinarides deformed differently along-strike during the Eo-Oligocene orogeny. To address these questions, we constructed a new 2D kinematic forward model traversing the central Velebit Mtn. across all tectonic units from the hinterland to the Adriatic foreland (Fig. 1c). For the construction of this model, we compiled and analysed local and regional stratigraphic variations to identify potential detachment horizons. In particular, we studied and simulated the influence of Mesozoic normal faults on the Cenozoic and present day structural architecture in this part of the External Dinarides.

In addition, we have revised instrumentally recorded seismicity in the wider Velebit Mtn. area, which is characterized by a relatively low seismic moment release (Ustaszewski et al., 2014); recorded maximal magnitudes are up to two magnitudes lower than in the rest of the External Dinarides (e.g. Schmitz et al., 2020; Petersen et al., 2021; Bagagli et al., 2022). The seismicity projected into our two regional cross-sections across the central and southern part of the Velebit Mtn. and its neighbouring areas shows a reasonably good correlation with the forward modelled subsurface fault geometries. This indicates that the 2D kinematic modelling approach can be used not only to assess subsurface fault geometries, but also that the latter provides a template to evaluate which faults presently form active seismogenic sources in the central External Dinarides.

### 1.1 Tectonic setting of the External Dinarides fold-and-thrust belt

The Dinarides fold-and-thrust belt formed along the eastern margin of the Adria microplate due to its convergence with the Eurasian plate since the Mid-Jurassic times (e.g. Schmid et al., 2020 with references). The fold-and-thrust belt extends for about 700 km in NW–SE direction from the Southern Alps in the north to the Dinarides-Hellenides transition zone in the south (Fig. 1a). In the northeast, the first-order tectonic boundary between the Adriatic- and European-derived tectonic units is known as the Sava suture zone

(Fig. 1c). This unit comprises subduction- to collision-related magmatic, metamorphic and flysch-type sedimentary rocks of Upper Cretaceous to Paleocene age (e.g. Pamić et al., 2002; Ustaszewski et al., 2009; Schmid et al., 2020). Classically, the Dinarides are subdivided into an external and an internal belt (Schmid et al., 2020). The external belt consists mainly of deformed Mesozoic shallow-marine carbonates of the Adriatic carbonate platform (Vlahović et al., 2005) and Cenozoic foreland basin deposits (e.g. Gobo et al., 2020). The internal belt additionally comprises Triassic to Mid-Jurassic ophiolites, ophiolitic mélange, deep-marine flysch-type sediments and metamorphic Paleozoic to Mesozoic basement, which together form three composite nappes that passively carry previously obducted ophiolites (Fig. 1c, for details see Schmid et al., 2020). These ophiolites, termed West Vardar ophiolites, were obducted during Middle to Late Jurassic times onto the eastern Adriatic plate margin (Robertson et al., 2009). The closure of Neotethys along the Sava suture zone during the latest Cretaceous to Paleocene (Ustaszewski et al., 2010) led to the formation of a SW-propagating nappe stack that reached the Adriatic carbonate platform in Early to Middle Eocene times and resulted in later formation of the External Dinarides fold-thrust belt (Dragičević et al., 1985, 1992; Schmid et al., 2020).

The Eo-Oligocene Dinaric orogeny led to the subdivision of the External Dinarides into three tectonic units: The High Karst unit, the Dalmatian unit and the undeformed Adria foreland (Fig. 1c; Schmid et al., 2020). Based on the two regional-scale balanced cross-sections, the High Karst unit was recently subdivided by Balling et al. (2021b) into the Upper and Lower High Karst subunits (Fig. 1c–e). They showed that during a first phase of crustal shortening the High Karst unit was internally thrust within the northeastern hinterland (Fig. 1d, e). Mechanically weak Permian evaporites served as the main detachment (Fig. 1d, e).

Following this internal thrusting of the High Karst unit, the subsequent deformation in the External Dinarides along the Split cross-section (Fig. 1e) propagated outward towards the SSW, at first along an up-stepping Lower Triassic siliciclastic detachment outcropping as the E-W striking frontal ramp of the Split-Karlovac Fault. Further SW at the contact between High Karst and Dalmatian units, the detachment ramped up into the Lower Cretaceous, which caused shortening in the Cretaceous to Eocene rocks of the Dalmatian unit. Consequently, the Split cross-section portrays a thin-skinned, in-sequence SW-propagating style of deformation along a stepped detachment. This is a deformation style that is observed in most foreland fold-and-thrust belts (e.g. Boyer & Elliott, 1982).



In contrast, along the Southern Velebit cross-section (Fig. 1d), the first internal shortening of the High Karst unit was transferred further SW along a detachment at the base of the Lower Cretaceous; shortening was first exclusively accommodated by thrusting in the Cretaceous and Eocene–Oligocene succession of the Dalmatian unit. This resulted in rather tight folding and thrusting in the southwestern frontal part of the cross-section (Fig. 1d). Subsequent shortening was related to the formation of a thick-skinned triangle structure in the southern part of the Velebit Mtn. (Fig. 1d). The lower part of this structure is composed of four thick-skinned SW-vergent duplexes, which are detached within the (pre-?) Paleozoic Adriatic basement at a depth of 15 km. The upper part of this structure is characterized by one major backthrust, i.e., the Lika backthrust, plausibly an inverted Mesozoic normal fault (Fig. 1d). Along the Lika backthrust, the entire Mesozoic carbonate platform sequence was thrust to the NE along a detachment within the Paleozoic basement (Fig. 1d). This style of deformation in the southern part of the Velebit Mtn. not only prevented further SW-propagation of the deformation front towards the foreland, but it also marks a distinct contrast to the along-strike deformational style observed along the Split cross-section (Fig. 1e).

As a result of this unique style of deformation, the Velebit Mtn. forms the most prominent geomorphic structure in the central part of the External Dinarides, extending for about 145 km in the NW–SE direction (Fig. 1b, c). Its highest peaks slightly exceed 1700 m a.s.l. and form a topographic barrier between the Adriatic coast and the Lika Plateau, a karst polje at an average elevation of 560 m a.s.l. (Fig. 1b). A rather complex geological structure of the mountain is composed of at least seven km-scale and asymmetric anticlines bounded along their NE limbs by faults here assigned to the Velebit Fault System (Fig. 2). On the Basic Geological Map of former Yugoslavia, sheets Otočac (Velić et al., 1974), Gospić (Sokač et al., 1974), Udbina (Šušnjar et al., 1973) and Obrovac (Ivanović et al., 1973), the faults of the Velebit Fault System were interpreted with a normal, top-NE offset, presumably overprinting previously formed anticline structures. However, in this study we challenge this interpretation by proposing that faults of the Velebit Fault System, together with faults of the Plitvice Fault System, as delineated in the Basic Geological Map sheet Bihać (Polšak et al., 1976), are Mesozoic extensional faults inverted into NE-vergent backthrusts during the main Eo-Oligocene shortening phase (Fig. 2).

The end of Paleogene orogeny of the External Dinarides is dated by the deposition of the Promina Beds in late Oligocene times in the western foreland (Zupanić & Babić, 2011). The Neogene opening of the Pannonian

Basin (Horváth et al., 2015) was associated with prominent extension in the Internal Dinarides (Andrić et al., 2017) and subordinately also the External Dinarides (Žibret & Vrabec, 2016; van Unen et al., 2019). In the latest Miocene contractional deformation affected the southern Dinarides (Handy et al., 2019; van Unen et al., 2019). The preservation of Oligo-Miocene marine terraces in the most external Dinarides suggest only minor Neogene deformation (Balling et al., 2021a).

## 2 From rifting to thrusting in the NE Adriatic margin: lithostratigraphy of the central External Dinarides

The study area is mainly built up by Mesozoic carbonate platform rocks (Fig. 2, compiled from the Basic Geological Map sheets of former Yugoslavia on the 1:100,000 scale; for references see figure captions). These are underlain by locally exposed Carboniferous to Permian and overlain by Eocene–Oligocene deposits, the latter mostly exposed along the SW margin of the Lika Plateau, along the SW slope of the Velebit Mtn. and its foreland, comprising the NW Dalmatian islands and the Ravni Kotari area (Fig. 2). The Miocene deposits crop out at the NE margin of the study area around Bihać, partly following the NE–SE strike of the Split-Karlovac Fault, and locally on the NE coast of the Pag island. The youngest deposits are of Quaternary age outcropping in numerous karst poljes on islands, in the coastal area and in the hinterland to the NE of the Velebit Mtn.

In the following, we summarize the main lithofacies characteristics of stratigraphic units shown on the geological map in Fig. 2. Based on compiled data from the Basic Geological Map sheets, literature, and deep boreholes, we evaluate lithofacies and thickness variations of stratigraphic units mapped in structural domains of the study area bounded by faults delineated in Fig. 2. This compilation is used to support preliminary assumptions regarding (i) the mechanical stratigraphy of particular stratigraphic units, (ii) the depth of possible detachment horizons, and (iii) the spatial distribution of lithofacies and their thickness variations, possibly controlled by pre-contractional fault structures. This information is utilized for the 2D kinematic forward modelling of the Central Velebit cross-section. For this purpose, the stratigraphic units presented in Fig. 2 are subdivided into five groups of depositional sequences related to particular phases of the tectonic and sedimentary evolution of the External Dinarides. The following subchapters provide descriptions of distinguished depositional sequences, the spatial distribution of lithofacies and their thickness variations, supplemented by schematic stratigraphic columns shown in Figs. 2, 3 and 4.

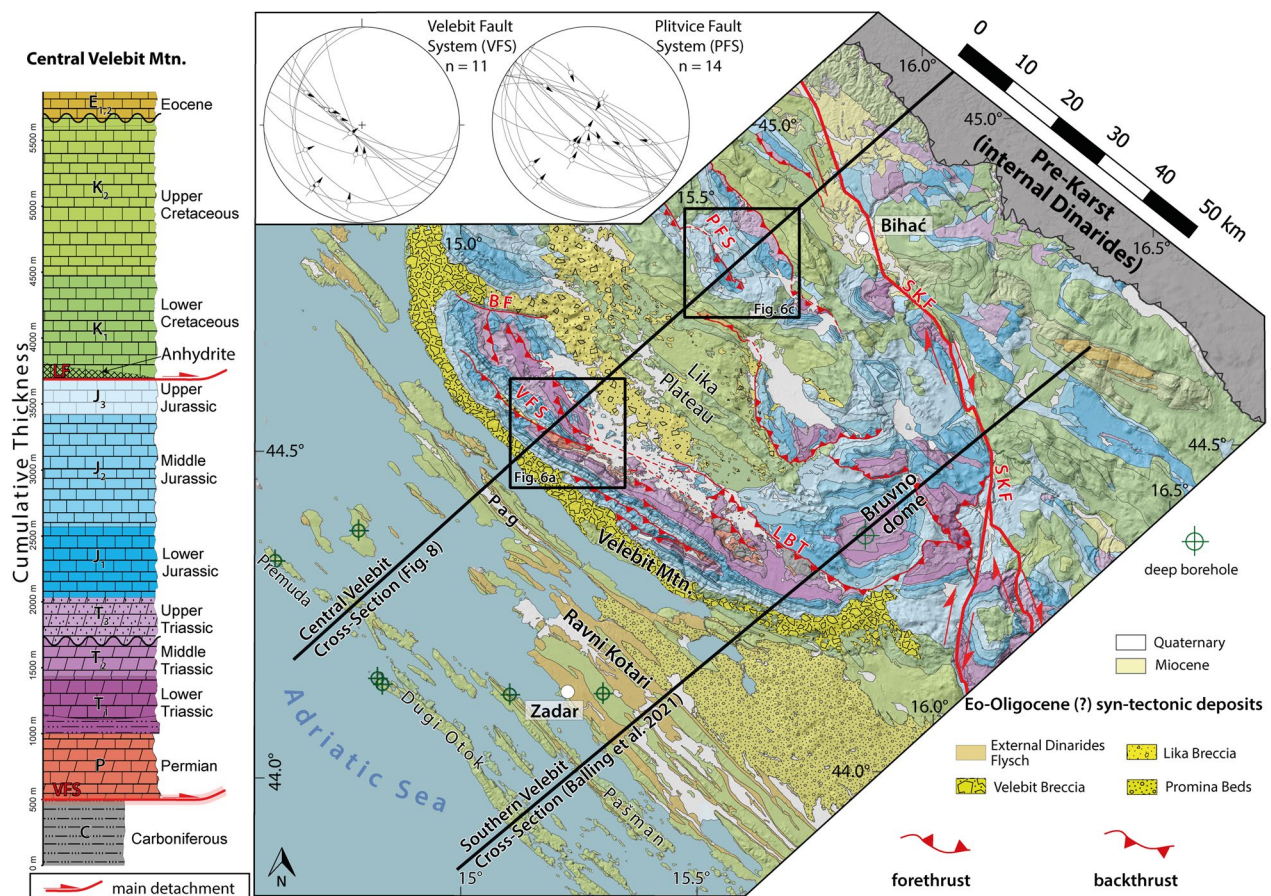


**Fig. 2** Geological map of the study area compiled from the basic Geological Maps of former Yugoslavia on the 1:100,000 scale, sheets Rab (Mamužić et al., 1969), Otočac (Velić et al., 1974), Bihać (Polšak et al., 1976), Bosanska Krupa (Mojčević et al., 1977), Silba (Mamužić et al., 1970b), Gospić (Sokač et al., 1974), Udbina (Šušnjar et al., 1973), Drvar (Šušnjar & Bukovac, 1978), Molat (Mamužić et al., 1970a), Zadar (Majcen et al., 1970), Obrovac (Ivanović et al., 1973), Knin (Grimani et al., 1972), Biograd (Mamužić & Nedela-Devide, 1968), Šibenik (Mamužić, 1971). The sense of slip of delineated faults in the Plitvice Fault System (PFS), Velebit Fault System (VFS) differs from the Basic Geological Map sheets. The Inset in the upper left shows stereoplots (equal-area, lower-hemisphere-projections) of fault-kinematic data reported from the Velebit and Plitvice Fault Systems by Balling et al. (2021b) and Krnjak (2019). Two NE-SW-trending trace show locations of the Central Velebit cross-section (Figs. 5, 8, 10) and the Southern Velebit cross-section [Figs. 1d and 11, modified after Balling et al. (2021b)]. The stratigraphic column on the left shows the generalized pre-deformational lithologies of the Central Velebit cross-section, comprising the homogenized thicknesses and the main detachments, located within the Carboniferous and at the base of the Lower Cretaceous strata. BF Bakovac Fault, LF Lika Flat, LBT Lika Backthrust

## 2.1 Adriatic pre-rift basement (Paleozoic)

The oldest exposed rocks in the central External Dinarides are Upper Carboniferous siliciclastic sandstones and shales, locally intercalated with subordinate quartzite-bearing conglomerates and fossiliferous limestones. These deposits crop out in the hanging wall of the Lika backthrust extending from the southeastern to the central part of the Velebit Mtn. (LBT, Fig. 2) and in its foot-wall within a core of the Brvno dome (Fig. 2; Šušnjar et al., 1973). Here, a 3.384 m deep borehole penetrated first through c. 250 m of Middle Triassic dolomites and clastics, and then through Carboniferous siliciclastic coarse- to fine-grained sandstones and siltstones interbedded with shales and limestones (Fig. 3; Šušnjar et al.,

1973). Therefore, beside rare lenses of limestones and conglomerates, the lithostratigraphy of the Upper Carboniferous unit is characterized here by prevalence of sandstones and siltstones, thus considered as mechanically rather uniform and noncompetent unit, representing the Adriatic pre-rift basement.

## 2.2 Neotethys syn-rift sequence (Permian–Middle Triassic)

The schematic lithostratigraphic logs from five areas along-strike the central External Dinarides document a lithofacies variation of the exposed Permian sedimentary sequence, deposited on the northern passive continental margin of Gondwana (Fig. 3; Vlahović et al., 2005). Northwest of the Split-Karlovac Fault the Lower Permian

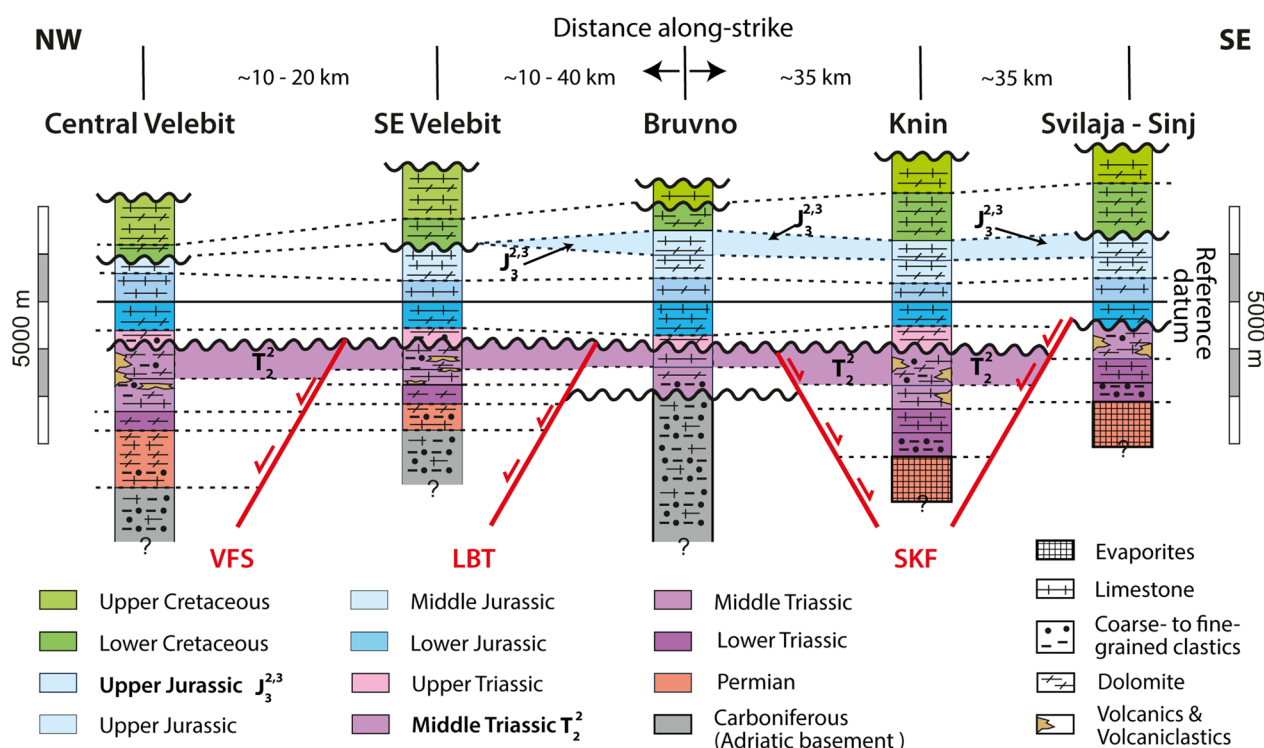


**Fig. 3** Schematic lithostratigraphic logs illustrating the along-strike facies changes in the sedimentary record of the External Dinarides in broader Velebit region. This correlation is based on five stratigraphic logs (locations can be found in Fig. 4), homogenized for smaller areas arranged across-strike, compiled from official geological map sheets (Grimani et al., 1972; Sokač et al., 1974; Šušnjar et al., 1973). The contact of Middle and Lower Jurassic was used as a reference datum. The correlation shows that the Split-Karlovac Fault served a paleogeographic boundary for the Upper Permian evaporites, which are exclusively preserved east of the fault. The preserved thickness of the upper Middle Triassic succession ( $T_2^2$ ) suggest that the area was affected by Mesozoic extension, dissecting the area from W-E into the Velebit half grabens, the Bruvno horst and the Knin graben. Combined with the present-day fault pattern it suggests that the Velebit backthrusts (Velebit Fault System, Lika Backthrust) and the dextral transpressive Split-Karlovac Fault originated from Triassic normal faults. Also the uppermost Jurassic ( $J_3^{2,3}$ ) shows a lateral facies pinchout towards the NW. The highlighted upper Middle Triassic and uppermost Jurassic successions, served as marker horizon to quantify and model the passive margin extension

is characterized by an alternation of limestones and sandstones, continuous and concordant with the underlying Carboniferous strata (Sokač et al., 1974). Locally the Carboniferous is unconformably overlain by Middle Permian sandstones and conglomerates, that grade upwards into coarse- to fine-grained sandstones and finally into limestones and dolomites of Middle and Upper Permian age (Fio et al., 2010). The Upper Permian dolomites crop out in a hanging wall of yet another backthrust outcropping to the SW of the Lika backthrust (Fig. 2; structural domain SD3 in Šrodoň et al., 2018). The thickness of the Permian succession in the Velebit Mtn. is highly variable along-strike (Fig. 3). In the central Velebit a thickness of 1.2 km is reported (Sokač et al., 1974), whereas in the southeastern Velebit the thickness is reduced to 500 m (Šušnjar et al., 1973). Further to the east at the Bruvno dome, the Permian was either not deposited or is not preserved (Šušnjar et al., 1973). Still further east in the Knin area, a minimal thickness of 500 m is reported for

Permian sediments (Grimani et al., 1972). Here the Permian is characterized by Upper Permian sabkha evaporites (gypsum, anhydrite, laminated carbonates, and rauhwacke; Kulušić & Borojević Šostarić, 2014), outcropping in form of salt diapirs along and to the east of the N-S striking segment of the Split-Karlovac Fault (Figs. 3, 4). Consequently, this fault has been interpreted to mark a boundary between two paleogeographic domains in the Permian: the northeastern domain characterized by deposition of evaporites, and the southwestern domain characterized by deposition of clastics and carbonates (Grandić, 1974; Šušnjar et al., 1992; Tišljar, 1992). In Permian times both domains were separated by the Bruvno dome in a paleogeographical horst position (Fig. 3). The associated Permian extension was most probably accommodated by SW- and ENE-dipping normal faults corresponding to the Lika backthrust, the Velebit Fault System and the Split-Karlovac Fault (Fig. 3). Due to the lack of evaporites in a close vicinity of the Velebit Fault



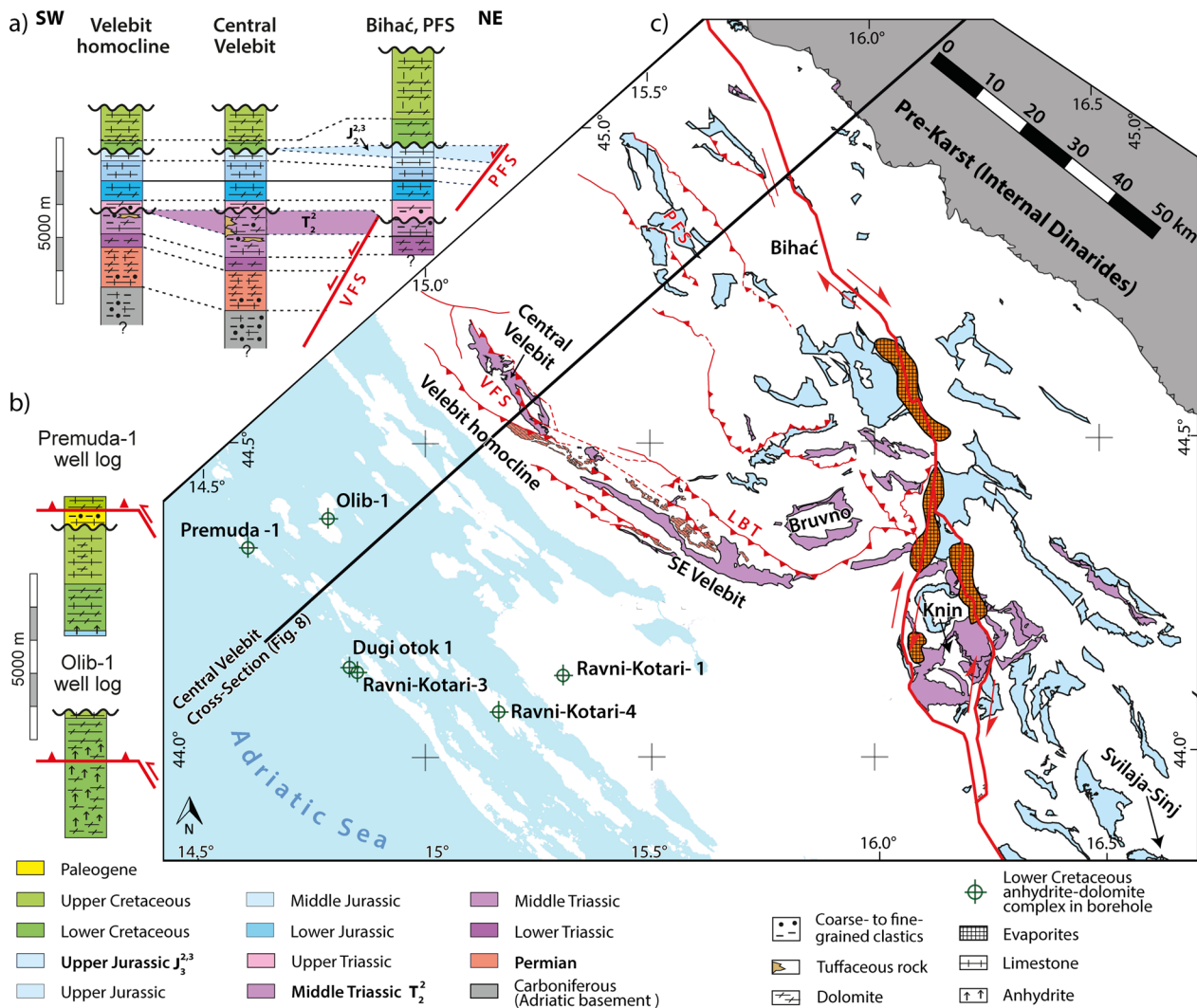


**Fig. 4** **a** Lithostratigraphic logs (Polšak et al., 1976; Sokač et al., 1974) showing the along-strike variations in the facies distributions along the Central Velebit cross-section. Highlighted are the upper sequence of the Middle Triassic ( $T_2^2$ ) and the Upper Jurassic ( $J_3^{2,3}$ ), both show a pinch out towards the SW. **b** Shows two bore logs from the Velebit foreland. The Premuda-1 borehole shows that Cretaceous is thrust on top a Paleogene succession and the presence of Lower Cretaceous anhydrite dolomite complex. The Olib-1 bore log shows a thrust within the Lower Cretaceous. **c** A simplified geological map showing the distribution of the Permian, Middle Triassic and Upper Jurassic successions. The Triassic and the Jurassic successions inferred to have been deposited in isolated fault-bounded basins, resulting in local depocenters, whereas the change in the Permian succession is related to a gradual change in the depositional environment, from up to 1200 m thick Permian clastic to carbonatic succession exclusively exposed in Velebit (Ivanović et al., 1973; Sokač et al., 1974) to the Upper Permian evaporites exclusively found along the Split-Karlovac Fault (Grimani et al., 1972; Tišljarić et al., 1998). An up to 700 m thick Middle Triassic sequence, consisting of limestones and volcanoclastic rocks (Pamić, 1984; Sokač et al., 1974), is exposed along strike of the Lika Backthrust (LBT), but pinches out to the northwest (**c**), becoming confined to the hanging wall of the two northern backthrusts of Velebit Fault System (Fig. 3a). Middle Triassic is also exposed around the Bruvno dome and in the hanging wall of the SW-vergent northern forethrusts. The up to 800 m thick Upper Jurassic carbonate sequence is exclusively exposed in the northeastern part of the study area. Most of the exposures are located around the Split-Karlovac Fault and Plitvice Fault System; a minority is exposed northeast of the Bruvno dome. LFS Lika Fault System, PFS Plitvice Fault System, LBT Lika Backthrust, SKF Split-Karlovac Fault

System and the Lika backthrust (Figs. 3, 4), the existence of a weak evaporitic Permian detachment horizon was excluded for the 2D kinematic forward modelling of the frontal southwestern part of the Central Velebit cross-section. Consequently, the Permian was treated as a mechanically strong layer in contrast to the weak and

ductile evaporite layer northeast of the Split-Karlovac Fault.

A similar variation in lithofacies and thickness is also documented for the Lower Triassic deposits (Fig. 3). The Lower Triassic strata are missing in the Bruvno dome, being either not deposited or eroded before the onset of

Middle Triassic deposition. To the west of the Bruvno in the central and southeastern Velebit area, the Lower Triassic is characterized by sandy dolomites concordant to Upper Permian dolomites (Fio et al., 2010). The thickness of Lower Triassic dolomites is estimated here to c. 400 m (Fig. 3; Sokač et al., 1974). To the east of the Bruvno dome, Lower Triassic deposits are exposed in the Knin and Svilaja–Sinj areas, here outcropping within the Split-Karlovac Fault zone and locally on top of Upper Permian evaporites (Grimani et al., 1972). The Lower Triassic succession comprises dolomites, red-coloured siliciclastics and limestones in a thickness of c. 800–1000 m (e.g. Aljinović et al., 2018). Assuming a non-deposition of the Lower Triassic strata in the Bruvno area, the compiled data suggest that the Bruvno dome was also in a horst position during Early Triassic times (Fig. 3). The thickness variations of the Lower Triassic northeast and southwest of the Split-Karlovac Fault, controlled by SW- and ENE-dipping normal faults, additionally support our interpretation that the Permian extension continued during Early Triassic times (Fig. 3).

The Middle Triassic (Anisian to Ladinian) at the Bruvno dome starts with coarse- to fine-grained clastics unconformably over Upper Carboniferous clastics, followed by dolomites and limestones. Here, the preserved thickness of Middle Triassic deposits is c. 1000 m (Fig. 3). In the area surrounding the Bruvno dome, the Middle Triassic deposits are continuous and concordant with underlying Lower Triassic carbonates, at first characterized by carbonates followed upward by a continuous succession of alternating volcanics, volcanoclastics and limestones. This succession was biostratigraphically dated to Upper Anisian - Ladinian (Figs. 3 and 4; Šćavničar et al., 1984; Smirčić et al., 2018, 2020). The across- and along strike variations in the preserved thickness of the Ladinian (upper part of the Middle Triassic succession), indicated as  $T_2^2$  and highlighted in purple in Figs. 3, 4a, are recorded by the stratigraphic logs and their present-day distribution in map view (Figs. 3, 4). The thickest preserved Middle Triassic succession is documented in the central Velebit, where it reaches 1400 m (Sokač et al., 1974). In the Knin area the Middle Triassic has a preserved thickness of 1300 m (Grimani et al., 1972) and in the Svilaja-Sinj area a thickness of 600 m (Šiftar, 1986). However, the geological map shows a condensed Ladinian unit in the Velebit homocline and in the Bihać area (Figs. 3, 4a).

The Middle Triassic succession of alternating limestones and volcanoclastics, locally basalts and andesites, is widespread in the External Dinarides fold-and-thrust belt. Magmatism was interpreted as related to the break-up of Adria in Middle Triassic times (Pamić, 1984; Smirčić et al., 2020). Middle Triassic continental rifting

accommodated by normal faults led to extension and formation of diversified marine environments and half-grabens (Lawrence et al., 1995).

A regional Middle Triassic extensional phase related to the formation of grabens and half-grabens best explains the thickness variations of the upper sequence of the Middle Triassic succession (Figs. 3, 4a). The schematic along-strike correlation of the Permian–Middle Triassic syn-rift deposits shown in Fig. 3 suggests the formation of the “Knin graben”, the “Bruvno horst” and the Middle Triassic half grabens in the Velebit area corresponding with the hanging walls of the Velebit Fault System faults (Fig. 4b). To account for this regional extensional event plausible basement-involved normal fault geometries were included in the 2D kinematic forward modelling approach, to account for the interpreted syn-rift deposition of the upper Middle Triassic succession (Smirčić et al., 2018, 2020).

### 2.3 Post-rift carbonate platform sequence (Upper Triassic–Cretaceous)

The Upper Triassic (Norian) dolomites (Hauptdolomit) were uniformly deposited across the Adriatic carbonate platform, locally preceded by a Carnian emersion phase characterized by bauxite and clastic deposits. The carbonatic successions of Lower and Middle Jurassic age of the Adriatic carbonate platform are preserved in rather uniform thickness across the study area and only local short-lasting emersion phases are reported (Vlahović et al., 2005). This contrasts with the Upper Jurassic (Kimmeridgian) partly deep water limestones, which again show differences in depositional facies and preserved thickness, related to changes in the water depth on a regional scale (Velić et al., 2002). Vlahović et al. (2005) interpreted these variations as indirect consequences of the first contractional tectonics recorded in the Internal Dinarides, contemporaneous with the obduction of the West Vardar Ophiolites onto the eastern Adriatic plate margin during Late Jurassic times (Robertson et al., 2009).

The exposed Latest Jurassic deep water carbonates ( $J_3^{2,3}$ ) known as the Lemeš unit of the External Dinarides (e.g. Velić et al., 2002; Vlahović et al., 2005; Vitzthum et al., 2022) are exclusively found in the northeastern half of the study area (Fig. 4c). The largest exposures of this unit within the study area are located with the area of the Plitvice Fault System and north and south of the Split-Karlovac Fault. Smaller patches of this unit crop out north of the Bruvno dome, which mark its southernmost exposure in the study area to the west of the Split-Karlovac Fault (Fig. 4c). Further to the southeast the exposures of the Lemeš unit follow the Split-Karlovac Fault (Velić et al., 2002). This unit is missing within the

exposed stratigraphy of the Velebit Homocline (Fig. 4a). This unit shows a maximum thickness of 600 m within the Plitvice Fault System (Fig. 4a), while Vitzthum et al. (2022) reported a maximum thickness of 450 m from the east of the study area. The Lemeš unit is interpreted as a Late Jurassic syn-tectonic unit (Velić et al., 2002; Bucković et al., 2004; Vlahović et al., 2005; Bucković & Markić, 2016). The correlation of the lithostratigraphic logs (Figs. 3, 4a) shows that the preserved thickness of the Upper Jurassic unit varies along-and across strike. However, it is still a matter of debate if this unit was deposited in an extensional or compressional setting. Consequently, both scenarios were tested during the 2D kinematic forward modelling approach in this study.

In the Early Cretaceous the Adriatic carbonate platform grew rather steadily, and no significant deformation events are known. The Lower Cretaceous comprises anhydrite-dolomite complex found in drill cores SW of the Velebit Mtn. (Figs. 2b, 4; Šiftar, 1982). This complex is dated as Lower Cretaceous (in Olib-1 and Premuda-1 boreholes; Tončić-Gregl & Prpić, 1971; Šiftar, 1982), and is also preserved at the boundary between Lower and Upper Cretaceous (Albian-Cenomanian) in the Ravni Kotari-3 and Dugi Otok-1 boreholes (Tončić-Gregl & Prpić, 1971). The presence of the Lower Cretaceous anhydrite-dolomite complex was considered as mechanically weak horizon and thus as a potential detachment in the 2D kinematic forward modelling approach.

The regionally widespread Aptian emersion phase in the Adriatic carbonate platform only had local implications on the preservation of Lower Cretaceous limestones (Vlahović et al., 2005), which led to thickness variations. The thickness distribution of the Upper Cretaceous carbonates was controlled by the interplay of eustatic sea level variations, local syn-sedimentary deformation (Prtoljan et al., 2007; Tišljarić et al., 1998) and vast amounts of carbonates by rudist growth (Vlahović et al., 2005). The subsequent Late Cretaceous to Paleogene emersion phase in the Adriatic carbonate platform, with only locally preserved successions of uppermost Cretaceous to Paleocene platform carbonates (e.g. Vlahović et al., 2005; Tešović et al., 2020), was followed by its drowning in Early to Middle Eocene time. This drowning was related to the flexural subsidence of the Adriatic foreland caused by the approaching orogenic deformation front that led to the formation of the External Dinarides foreland basin (Čosović et al., 2018).

#### 2.4 Syn-orogenic sequence (Middle Eocene–Oligocene)

The Middle–Upper Eocene External Dinarides flysch-type deposits and Eocene–Oligocene Promina Beds are considered as syn-orogenic deposits described in detail in e.g., Zupanić and Babić (2011), Mrinjek et al. (2012)

and in Balling et al. (2021b). The longest SW-dipping homocline exposed along the SW slope of Velebit Mtn. facing the Adriatic Sea (Fig. 2) is characterized by a belt of massive carbonate breccia presumably formed during the Paleogene and Neogene, which unconformably rests on top of SW-dipping Jurassic and Cretaceous strata (known as the Velebit breccia after Vlahović et al., 2012). Along the NE margin of the mountain and within the Lika Plateau yet another belt of carbonate breccia is widely exposed, known as the Jelar deposits (Bahun, 1974), which lies over Jurassic and Cretaceous carbonates (Fig. 2). In general, both belts of carbonate breccia are considered here as syn-orogenic although of different origin that is reflected in their structural position and clast composition: the Velebit breccia is mostly polymictic vs. the Jelar breccia is mostly monomictic.

#### 2.5 Post-orogenic sequence (Miocene lake sediments)

The Miocene lake sediments represent the most prominent post-orogenic sequence of the External Dinarides. Fresh water micritic limestones and marls locally associated with coal seams were deposited in isolated lakes comprising the Dinaride Lake System (e.g. de Leeuw et al., 2012). In the study area these rocks are exposed in the north around the city of Bihać and in the southwest on the Pag Island (Fig. 2). On this island, Miocene sediments are represented by alternating limestones, sandstones and marls with coal seams with an average dip of 15° towards the NE (Bulić & Jurišić-Polšak, 2009; Mamužić et al., 1970b), in contrast to the underlying Cretaceous carbonate platform and Eocene limestone and flysch-type deposits that are intensively folded in hanging walls of SW-verging thrust faults (Fig. 2). Based on paleomagnetic results obtained in Miocene sediments on Pag Island and those obtained in other basins of the Dinaride Lake System, de Leeuw et al. (2012) concluded that the Dinarides have not rotated since the deposition of these sediments.

### 3 Construction of a reference cross-section

The Basic Geological Map sheets Molat, Silba, Bihać, and Gospić (Mamužić et al., 1970a, 1970b; Sokač et al., 1974; Polšak et al., 1976) were used as the prime data sources during the construction of a new regional balanced cross-section across the Central Velebit Mtn. (see Fig. 1c for the trace of this section), providing data on bedding dip, lithological contacts and thickness of stratigraphic units (Figs. 3, 4a). This data source was supplemented by field observations and fault-kinematic measurements (Fig. 2). Based on these data, the kink-band method (Suppe, 1985) was used to construct a geological cross-section across the Central Velebit Mtn. (Fig. 5). This cross-section represents the present-day deformed state of the uppermost



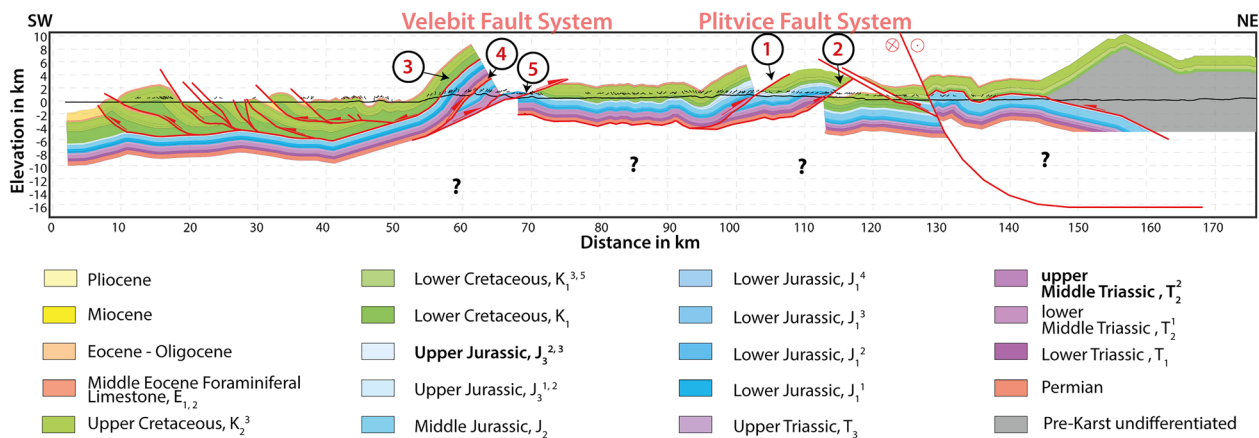


**Fig. 5** Reference Central Velebit cross-section, constructed by the kink-band method (Suppe, 1985) on the basis of bedding data and lithostratigraphic contacts taken from official geological maps. In combination with the lithostratigraphic logs (Figs. 3, 4) the thickness for each lithostratigraphic unit was extracted to setup a layer cake model. This cross-section served as a reference for the 2D kinematic forward model workflow. The Plitvice Fault System contains—Fault #1: Plitvice Fault, Fault #2: Lisina-Bačinovac; VFS Velebit Fault System contains Fault #3: Brušane-Oštarije Fault, Fault #4: Jadovno Fault, Fault #5: Bužim Fault

crust and served as a reference section for the 2D kinematic forward model approach.

The trace of the Central Velebit section runs SW–NE, perpendicular to most structures in the central part of the External Dinarides (Figs. 1, 2). In the SW, the cross-section runs across the NW Dalmatian islands from Premuda to Pag island. According to the Basic Geological Map sheets Molat (Mamužić et al., 1970a), Silba (Mamužić et al., 1970b), and Gospić (Sokač et al., 1974), the oldest exposed rocks in this area are Lower Cretaceous carbonates thrust on top of Upper Cretaceous carbonates and Eocene limestones and flysch-type deposits, resulting in a set of NW–SE striking and SW-verging fault-related folds, exposed at the surface as island anticlines (Figs. 2, 5).

Across the coastline and along the SW facing Velebit Mtn. slope, the cross-section cuts across the belt of occurrences of the Velebit Breccia (Vlahović et al., 2012) that in this part lies unconformably over Upper Jurassic and Lower Cretaceous carbonates (Fig. 2). Together with underlying and mostly concordant Lower and Middle Jurassic, Triassic and Permian strata, this breccia forms a homocline that corresponds with the SW-dipping limb of the Baške Oštarije anticline (Fig. 6). The NE limb of this anticline is cut and bounded by the Brušane-Oštarije (#5, Fig. 6) fault that, together with Jadovno (#4, Fig. 5) and Bužim (#3, Fig. 5) faults, comprises the Velebit Fault System (Figs. 2, 5, 6a). Fault-kinematic data measured along the Velebit Fault System indicate top to the NE tectonic transport (Balling et al., 2021b, Fig. 2b). Combined with data from the Basic Geological Map sheet Gospić (Sokač et al., 1974), we

propose that the Velebit Fault System here consists of three steeply SW-dipping backthrusts (Figs. 5, 6a). Further to the NE the cross-section runs across the Lika Plateau, exposing Lower and Upper Cretaceous carbonates at the surface, overlain by a carbonate breccia of presumably Eo-Oligocene age (Figs. 2, 5, 6a).

To the NE of the Lika Plateau, the cross-section portrays the Plitvice Fault System, first across the Lisina-Bačinovac (#2, Fig. 5) and then across the Plitvice Fault (#1, Fig. 5). The former thrusts Lower Jurassic onto Middle Jurassic carbonates; the latter thrusts Upper Triassic dolomite onto Upper Cretaceous carbonates, which is supported by kinematic data reported by Krnjak (2019) similar to those measured in the Velebit Fault System (Fig. 2).

Northeast of the Plitvice Fault, the section strikes across the Bihać freshwater basin, part of the Miocene Dinaride Lake System (e.g. de Leeuw et al., 2012). Here, according to the Basic Geological Map sheet Bihać (Polšak et al., 1976), the mostly flat lying Miocene strata seal a SW-vergent thrust fault, which brings Lower Cretaceous on top of Upper Cretaceous carbonates. The northern part of the Bihać Basin is affected by the Split-Karlovac Fault (SKE, Chorowicz, 1975), recently described by Balling et al. (2021b) as a dextral tear fault initiated during Eo-Oligocene deformation phase in the central External Dinarides. In the northeastern-most sector, the cross-section cuts across the High Karst/Pre-Karst tectonic boundary, i.e., the frontal thrust of the Pre-Karst nappe that brings Triassic clastics and carbonates on top of Upper Cretaceous-Paleocene flysch-type deposits (Korolija et al., 1979; Figs. 2, 5).

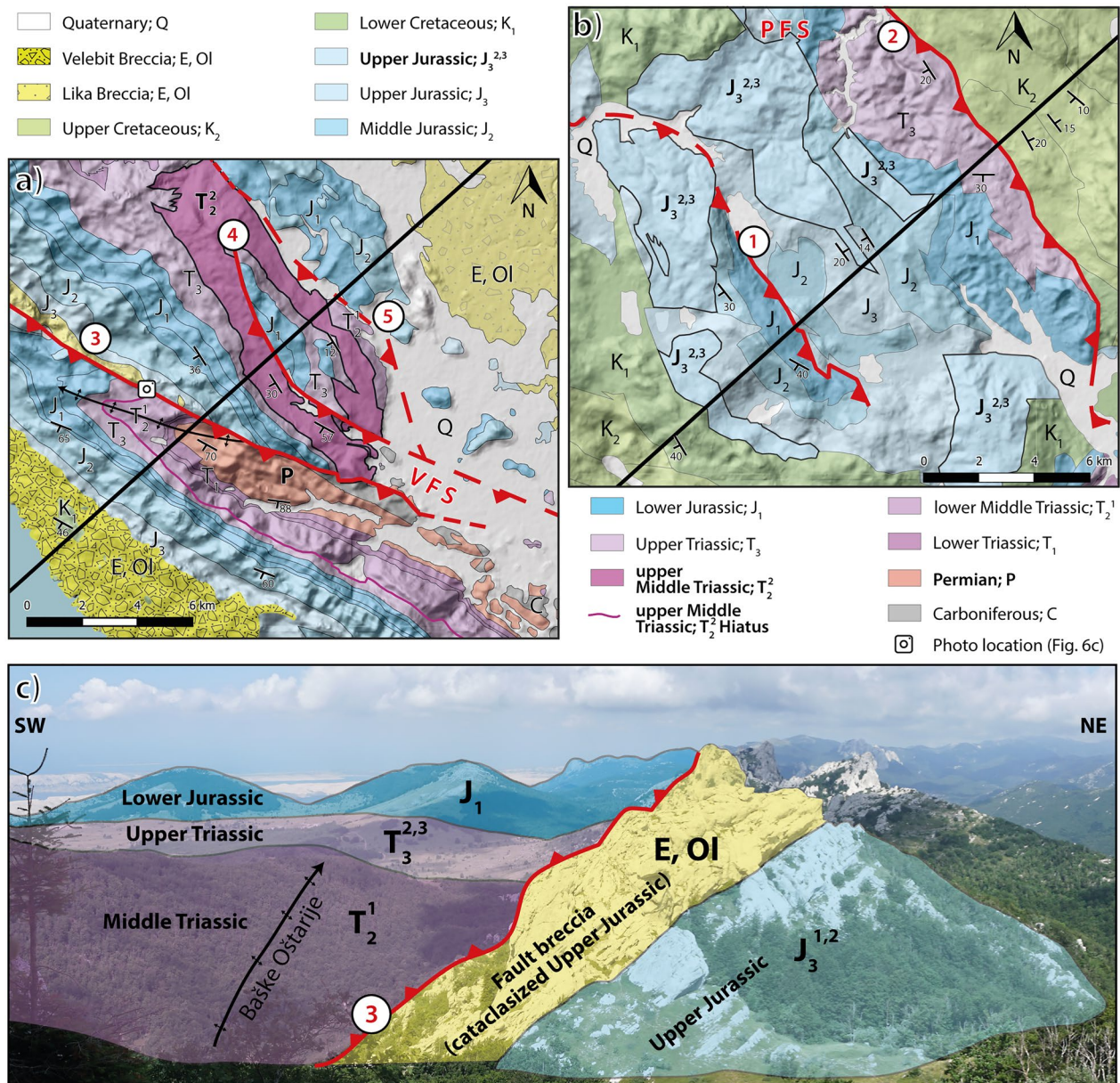


**Fig. 6** Detailed geological maps of two key locations, characterized by fault-bounded Mesozoic sedimentation preceding Cenozoic contraction. **a** Southern Velebit Fault System (VFS), **b** the Plitvice Fault System (PFS). NE-vergent backthrusts are numbered according to their relative initiation during the Eocene–Oligocene deformation: 1: Lisina-Bačinovac Fault, 2: Plitvice Fault, 3: Brušane-Oštarije Fault, 4: Jadovno Fault, 5: Bužim Fault. The black line marks the section trace of the Central Velebit cross-section (Fig. 8). The exact location of both areas can be found in Fig. 2. **a** Shows that the Middle Triassic unit T<sub>2</sub><sup>2</sup> (Ladinian) is missing in the hanging wall of Fault #3 (purple line). Figure 3b shows a detailed map of the PFS with the Upper Jurassic Lemeš formation (J<sub>3</sub><sup>2,3</sup>) being exclusively confined to the hanging walls of Faults 1 and 2. **c** Shows an annotated field photo of the top NE vergent Brušane-Oštarije Fault (#3) with the westward plunging anticline in the hanging wall and a Eo-Oligocene carbonatic fault breccia in its footwall. The breccia consists of reworked Upper Jurassic carbonate. In contrast to the Upper Jurassic, the bedding planes within the breccia are not preserved. See Fig. 5a for the photo location

### 3.1 Detailed view on two backthrust systems: the Velebit and Plitvice Fault Systems

To better understand the cause for the reported triangle structure in the Velebit Mtn. (Fig. 1d), a more

detailed understanding of the initiation of the Velebit and Plitvice Fault Systems is needed (Fig. 6). Figure 6a shows a zoom-in on the Velebit Fault System, modified after the Basic Geological Map data, sheet Gospić



(Sokač et al., 1974). This figure illustrates that the Velebit Fault System here consists of three backthrusts, all located within a distance of 6 km. The respective hanging walls of those three backthrusts of the Velebit Fault System are SW-dipping, with beddings dips progressively steepening towards the SW (Fig. 6a). Based on (i) the vicinity of the faults and (ii) the SW-directed steepening of the hanging walls, we presume that the faults of the Velebit Fault System were initiated successively from SW towards NE. This led to passive steepening of the early faults and their hanging walls. The southwestern most Brušane-Oštarije fault (fault #3 in Fig. 6a) seems to have initiated first, since it is the steepest fault. Thus, it is assumed that this fault was progressively tilted during the later movement along the Jadovno and Bužim faults (#4 and #5 in Fig. 6a, respectively). Across-strike the bedding of the hanging wall strata of these two faults shows a progressive inclination towards the SW. This supports the assumption of a NE propagation of the deformation front, leading to the formation of NE-vergent backthrusts of the Velebit Fault System. This hypothesis was tested and confirmed during the later 2D kinematic modelling approach. The hanging walls of the Plitvice Fault System (Fig. 6b) do not show a progressive inclination towards the SW. Most probably this is due to the fact that the distance between the two faults is too large to interfere. Consequently, a relative timing of the movement along the Plitvice Fault System is still not clear. However, a top to the NE transport direction and a NE-ward propagation of the two backthrusts of the Plitvice Fault System was assumed similar to the faults of the Velebit Fault System, which was also tested during the 2D kinematic modelling approach.

A field photo of the Brušane-Oštarije fault (Fig. 6c) illustrates a northwestward plunging anticline mapped in the hanging wall of this SW-dipping thrust fault (Fig. 6a; Sokač et al., 1974). The direct footwall of this fault is marked by a c. 20 m wide damage zone composed of a monomict carbonate breccia in cataclastically deformed Upper Jurassic limestones. Below the damage zone, SW-dipping bedding in these limestones is clearly preserved (Fig. 6c). Thus, we interpreted this damage zone as a cataclastic fault breccia, which extends along that section of the fault where carbonate rocks in its hanging wall (Middle Triassic to Upper Jurassic) and its footwall (Upper Jurassic) are juxtaposed. Sporadically, this fault breccia contains pockets of talus-like breccia comprising clasts of Lower-Middle Eocene Foraminifera limestones, thus indicating a possible age of faulting and breccia formation in Middle Eocene and Oligocene times, in agreement with the Basic Geological Map sheet Gospić (Fig. 6a, Sokač et al., 1974).

## 4 Methods

Two-dimensional kinematic forward models were used to constrain subsurface structure geometries in tectonically complex settings. These geometries are of fundamental value to assess the spatial distribution of crustal shortening and to study the structural evolution of an orogen. Based on a trial-and-error workflow (Fig. 7), the hanging wall geometries of individual faults and fault-related folds were modelled to resemble the deformed state cross-section (Fig. 5). Fault-specific parameters such as displacement and timing of deformation associated with single faults were assigned, changed, and improved during the forward modelling process. These small-scale model runs were combined with large-scale cross-sections in the central and SE part of the Velebit Mtn. (section trace Fig. 1c).

For this approach the software Move by Petroleum Experts was used. The reference cross-section (Fig. 5) was used for comparison with the kinematically forward modelled layer cake model. The initial layer cake model represents the undeformed state, where thickness information for every lithological unit was taken and harmonized from the reference cross-section, well logs, and the basic geological map sheets. During the kinematic forward modelling, the thickness of each stratigraphic unit was kept constant to satisfy balancing assumptions. The undeformed layer cake model served as a starting point for the second step forward modelling approach. To account for possible flexural subsidence due to the tectonic load of the orogenic wedge, a published cross-section (Amoco, 1990) was used to extract the depth of the base of the Permian, which was used as a marker bed. This depth information was supplemented by projected borehole data and used as a boundary condition for the layer cake model.

The undeformed layer cake model was kinematically forward modelled along individual faults during a trial-and-error approach (Fig. 7) to resemble the near surface geometry of the reference cross-section (Fig. 5). To achieve the best agreement between the deformed layer cake and the reference cross-section, curvature, dip, depth, and displacement along several possible faults were adjusted stepwise. For this, the compiled stratigraphy (Figs. 2, 3, 4a) was used to assess the depth and geometry of possible detachments. During more than one hundred iterations, various depths of the main detachment between 10 and 20 km depth were tested. Due to computational limitations this was done for every fault individually since it was only possible to model one fault at a time. It was assumed that all folds are fault-related, to obtain a balanced and restorable forward model. Based on the dip of the fore- and back-limbs and fault-kinematic data, different algorithms were used



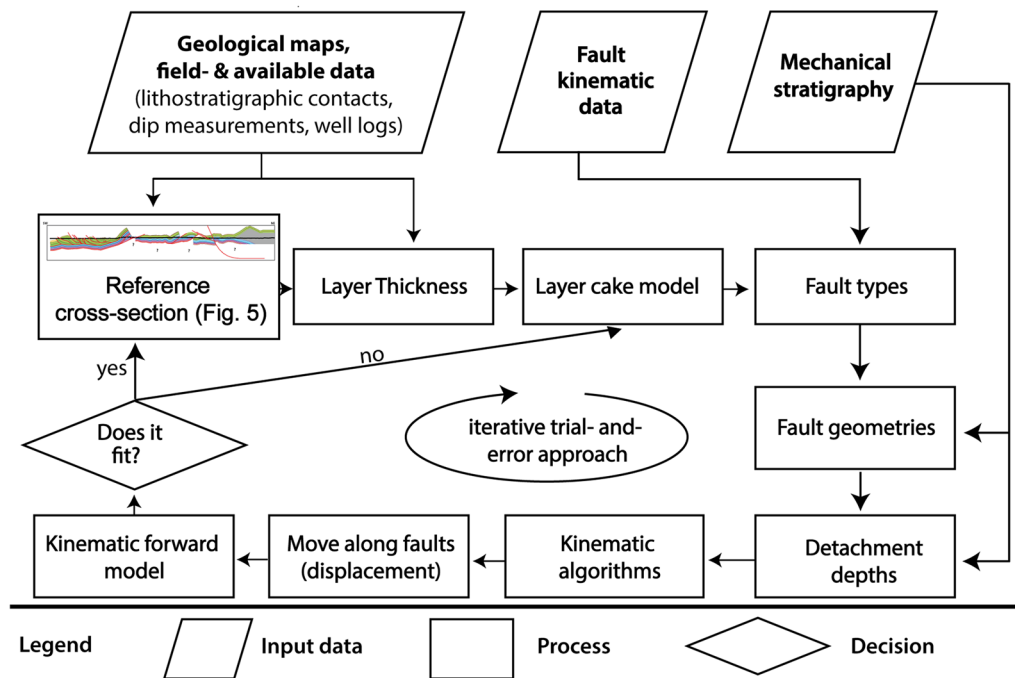


**Fig. 7** Workflow chart showing the procedure of 2D kinematic forward modelling. A reference profile, depicting present-day, deformed state geometries, is constructed 'ad hoc' based on available geological maps, field data, bedding information, or borehole logs. Information on stratigraphic thicknesses is extracted from the reference model. Using predefined kinematic algorithms, a stratigraphic template is then deformed in a trial-and-error approach to reproduce geometries of the reference profile. This iterative workflow solves for the best-fit between the kinematically deformed layer cake model and the reference profile

to achieve the best-fit subsurface geometry. For modelling the hanging wall geometries along normal faults, the *Simple Shear* algorithm (Verrall, 1981; Gibbs, 1983; Withjack & Peterson, 1993) was used. This algorithm yields the most realistic results in extensional regimes. For thrust faults the *Fault Parallel Flow* (Egan et al., 1997) and the *Fault Bend Fold* (Suppe, 1983) algorithms were applied. Both algorithms are best suited to forward and backward model contractional deformation. The *Fault Bend Fold* algorithm can only be applied to rather shallow thrusts ( $< 30^\circ$ ), whereas the *Fault Parallel Flow* algorithm yields kinematically viable results also for steeper thrusts ( $> 30^\circ$ ). However, both algorithms cannot be used to model overturned forelimbs above blind thrusts. In this case the *Fault Propagation Fold* (Suppe & Medwedeff, 1990) algorithm was utilized.

Different deformation scenarios were tested by running crude forward models to explore changes in the tectonic regime through time. During this stage, both a Middle Triassic and an Upper Jurassic extensional event were modelled, in order to account for the spatial distribution and the lateral facies transitions of the Mesozoic syn-rift sediments in the area (Figs. 3, 4). These intermediate forward modelling results were checked against the available constraints (outcrop patterns, borehole data as well as

dip and fault-kinematic data). The best-fit crude forward model was refined, and minor changes were applied to individual fault geometries and amounts of displacement along individual faults to better fit the deformed state reference profile (Fig. 6). The final input parameters can be found in Additional file 1.

## 5 Results

### 5.1 The Central Velebit cross-section

The central part of the best-fit kinematic forward model shown in Fig. 8a, b portrays a 75 km wide triangle zone between the Adriatic coast and the Split-Karlovac Fault, where Eo-Oligocene shortening was accommodated within two structural levels. The structurally lower level forms a blind antiformal stack, where the (pre-?) Paleozoic basement is detached at a depth of 15 km and stacked internally by five SW-propagating thrust imbricates or compressional duplexes. These duplexes caused the surface uplift of the Lika Plateau (Figs. 1c, 8a). In 4 km depth underneath the Lika Plateau the passive roof thrust (sensu Banks & Warburton, 1986) is located at the base of the Permian. Along this passive roof thrust the five NE-propagating fault splays are detached, forming the emerged backthrusts of the Velebit and the Plitvice imbricated fault systems (Velebit and Plitvice Fault

(See figure on next page.)

**Fig. 8** **a** Balanced and kinematically forward modelled central Velebit cross-section. The frontal SW part of the section is dominated by thin-skinned high frequency deformation of the Cretaceous and Eocene strata. The central part, comprising the Velebit mountain, Lika, and the Plitvice Fault, showing thick-skinned deformation of a blind SW-vergent duplex and a set of five NE-vergent backthrusts (numbered according to their relative initiation), forming a complex Velebit–Lika–Plitvice triangle zone. This triangle structure has its basal detachment in the Pre-Carboniferous basement. The passive roof thrust detachment is located within the Permian or Middle Triassic syn-rift sediments. The northern part is characterized by thin-skinned deformation (nappe stack) and thick-skinned deformation of the Pre-Karst, thrust on top of the High Karst. The northern segment is cut by the regional dextral transpressive Split-Karlovac Fault. **b–e** Show individual deformation steps of the kinematic forward modelling. The amount of crustal shortening for the High Karst and Dalmatian units here is 94 km. **c** Shows the partial retrodeformation of the LFS and **d** shows the retrodeformation of LFS and PFS and captures the first contractional deformation along the cross-section, showing the internal High Karst nappe stack and the frontal thin-skinned deformation. **e** Shows the initial undeformed layer cake model. Note that the modelled Mesozoic extension amounts to 4 km, illustrated in the frontal part of the restoration steps. For an animated version of this figure, see Additional file 2

Systems in Figs. 2 and 5, respectively). Our results show that four out of these five emerged backthrusts were initiated along inherited Middle Triassic and Late Jurassic basement involved normal faults (Fig. 8e). Within the Velebit Fault System, two SW-dipping Middle Triassic normal faults were inverted along their top-most parts as SW-dipping and NE-vergent backthrusts. The best-fit geometry for the Plitvice Fault System suggests that both backthrusts originated from Upper Jurassic SW-dipping normal faults. Consequently, the best fit-kinematic model documents that the inversion of the Mesozoic normal faults played an important role for the initiation of the Velebit-Lika-Plitvice triangle structure. Despite the fact that the Velebit-Lika-Plitvice triangle structure is built up by multiple fore- and backthrusts, it can be classified as Type-II ramp triangle structure as defined by von Hagke and Malz (2018).

In contrast to the thick-skinned dominated central part of the Central Velebit cross-section (Fig. 1d), the SW part of the section, the Velebit foreland, is exclusively characterized by thin-skinned tectonics. In this part of the cross-section, the best-fit kinematic model shows that Cretaceous and Eocene rocks are deformed by tight folding and thrusting exclusively during top SW tectonic transport. Here, the main detachment is located at a depth of 5.5–4 km at the base of the Lower Cretaceous, along the mechanically weak anhydrite-dolomite complex. This detachment decouples the Cretaceous and Eocene from older strata. This decoupling within the Mesozoic Carbonate Platform rocks is caused by the High Karst internal nappe stack in the northeastern part of the cross-section where the Permian evaporites are detached and thrust, together with the overlying strata, on top of the Upper Jurassic carbonates (Fig. 8d). As a geometric consequence, the excess of shortening in the Cretaceous and Eocene units in the northeastern part of the cross-section is transferred along the c.80 km long “Lika flat” and accommodated in the southwestern part of the cross-section by a set of SW-vergent fault related folds (Fig. 8d). The best-fit kinematic forward model

shows that the forelimb of the nappe stack was used as a ramp for the NE-vergent Plitvice backthrust (Fig. 8c).

The northeastern part of the cross-section is characterized by the presence of the dextral strike-slip Split-Karlovac Fault. In map view this part of the Split-Karlovac Fault is associated with exposures of the Permian evaporites (Figs. 3, 4a). Therefore, the balanced cross-section accounts for possible salt movements in the subsurface by the presence of salt pillow structures, locally leading to variable thickness of the Permian unit. At the northeastern termination of the cross-section the undifferentiated Pre-Karst unit is thrust on top of the High Karst units. The frontal thrust of the Pre-Karst unit shows a rather complex flat-ramp-flat-ramp-flat geometry and roots into the same main detachment as both the Split-Karlovac Fault and the compressional duplexes of the Velebit-Lika-Plitvice Triangle structure at a depth of 15 km (Fig. 8b).

## 5.2 Relative timing of deformation

Due to the complex geometry of the final kinematic forward model, relative timing of deformation has direct implications on both the modelled faults and their hanging wall geometries and thus on the entire structural architecture of the cross-section. Consequently, the relative timing of deformation is an important result of the trial-and-error workflow. Figure 8b–e display four deformation steps of the best-fit kinematic forward model (for better visualization, see the restoration animation, Additional file 2). The first modelled deformation phase is related to the Middle Triassic extensional phase, shown with the Mesozoic strata on top (Fig. 8e). Due to the movement along the two basement-involved normal faults, the two Middle Triassic half grabens formed, filled with syn-rift sediments and volcanics. Similarly, these were followed by modelled extension that took place in the Latest Jurassic times, along the two-basement involved normal faults that controlled the local deposition of the Lemeš unit.

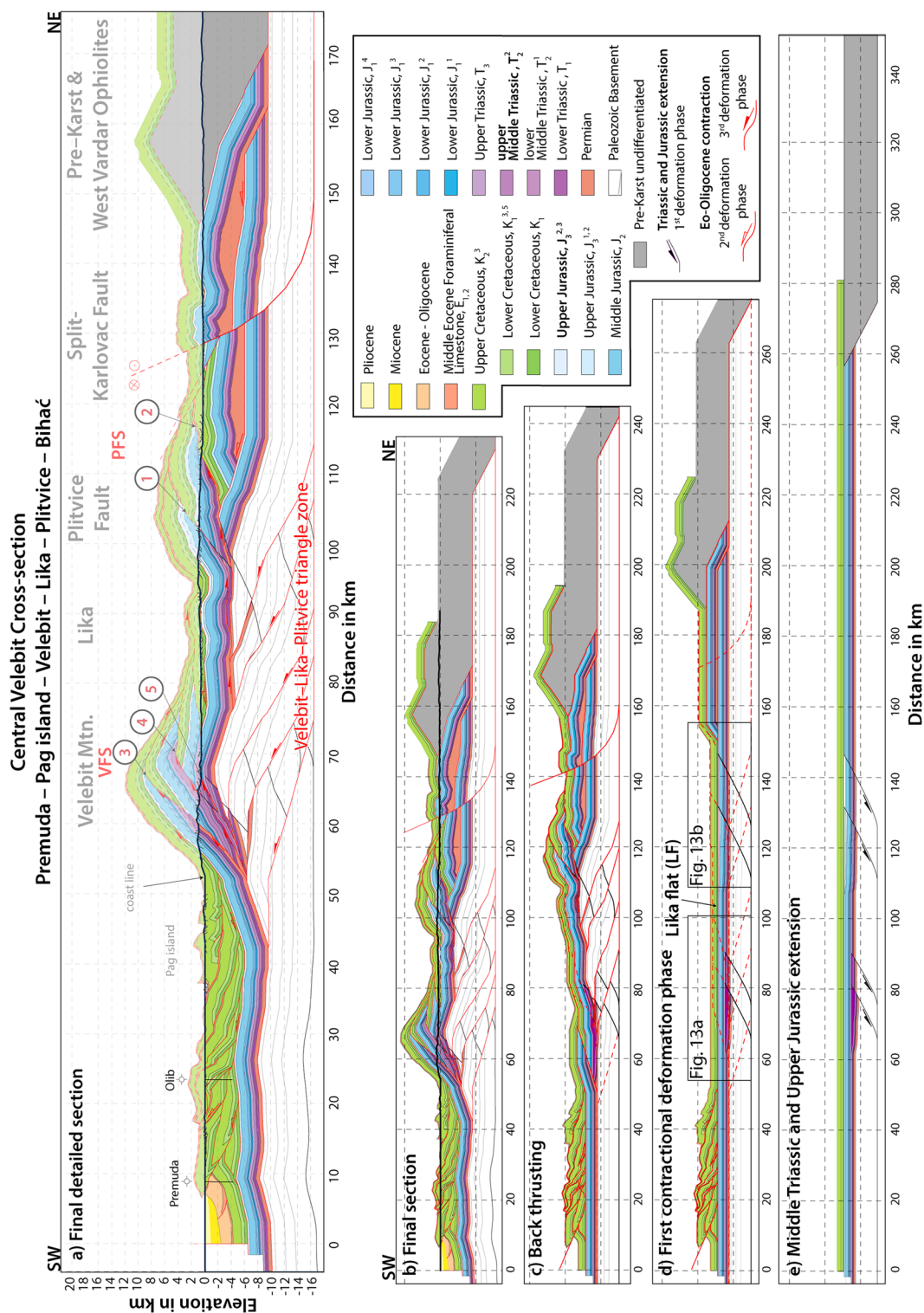


**Fig. 8** (See legend on previous page.)

Regarding the Eo-Oligocene shortening, the best-fit model suggests an overall outward propagation of the deformation front towards the SW. This is

best illustrated by the fact that the Pre-Karst unit was thrust first onto the High Karst unit in the NE (Fig. 8d, e). This thrusting took place before or during



the deposition of the Early–Middle-Eocene Foraminiferal Limestones and marks the first Cenozoic shortening event in the study area. Since then, the Pre-Karst unit was passively transported in a piggy-back fashion towards the SW, by internal nappe stack thrusting on top of the High Karst unit (Fig. 8d). Our results show that the internal flat-ramp-flat detachment geometry within the High Karst unit transferred further shortening to the southwestern-most part of the cross-section along the c. 80 km long Lika flat located at the base of the Lower Cretaceous within the anhydrite-dolomite complex (Fig. 8d). This led to thin-skinned folding and thrusting of the decoupled Cretaceous and Eocene units in this southwestern part of the cross-section.

The initiation of the Velebit-Lika-Plitvice triangle zone and the dextral Split-Karlovac Fault marks the youngest stage of horizontal shortening captured within the central part of the cross-section. According to the kinematic model, the Plitvice Fault System was established first on top of the SW-vergent blind thick-skinned compressional duplex (Fig. 8c). The outward propagation of this antiformal stack towards the SW led to the initiation of inversion of the Velebit Fault System. Although our results show an overall SW-propagation of the deformation front, a more detailed inspection of both the Plitvice Fault System and the Velebit Fault System suggest a NE-propagation of the individual emerged backthrusts. This is contrary to the theoretical model of a triangle zone formation proposed by von Hagke and Malz (2018) and initially by Banks and Warburton (1986). Both publications show a foreland propagating backthrust system.

Due to the along-strike contrasting styles of deformation in the External Dinarides presented in Balling et al. (2021b) (Fig. 1d, e), the movement along the Split-Karlovac Fault was modelled to take place contemporaneously with the formation of the Velebit-Lika-Plitvice triangle zone (Fig. 8). The Split-Karlovac Fault shows predominantly dextral strike-slip movement, which transported material out of the section plane. Nevertheless, our kinematic model suggests a vertical offset along the Split-Karlovac Fault of 2.7 km during the Eo-Oligocene shortening, which ended with the end of the deposition of the Promina Beds, dated to late Oligocene (Zupanić & Babić, 2011).

### 5.3 Seismicity

Seismicity within the greater Velebit area is considerably weaker than in most other parts of External Dinarides (Ustaszewski et al., 2014). Earthquakes are more common and seismic hazard is larger in the adjacent regions both to the NW (between Kvarner and Gorski Kotar) and the SE (Central Dalmatia, Fig. 9; Herak et al., 2011).

Historical records mention only few earthquakes that have caused damage in the Velebit and Lika areas. The strongest ones among them, all with estimated epicentral intensities of  $I_0 = \text{VII EMS}$  (corresponding to macroseismic magnitudes  $M_m$  between 4.7 and 5.3), occurred in central Lika in 1893 and 1959, and below the western foothills of central Velebit in 1949. A detailed insight into earthquake activity of the Velebit–Lika area has been provided only rather recently, when several broad-band digital seismographs were installed in the greater Velebit area in the first decade of the twenty-first century. Much more detailed coverage was obtained during the VELEBIT (Croatian Science Foundation, 2015–2018) and AlpArray (Molinari et al., 2016) projects, when additional temporary stations operated in the region. Recent seismicity is shown in Fig. 9 after data from the Croatian Earthquake Catalogue (CEC, Herak et al., 1996, updated until the end of 2020). It presents epicenters of earthquakes from the period 1995–2020, with local magnitude  $ML \geq 1.0$  and standard errors of the epicenter and focal depth of  $\sigma_E < 3$  km and  $\sigma_H < 4$  km, respectively. For this study, these earthquakes have been relocated in five iterations, each consisting of computation of hypocentral locations followed by estimation of source-specific station corrections (see Herak and Herak, 2021, for details of the procedure). Probable quarry blasts were removed from the final catalogue. Figure 9 also shows the Focal Mechanism Solutions (FMS) from the corresponding Croatian FMS-database (Archives of the Department of Geophysics in Zagreb) for the years 1995–2021. Solutions for earlier events are not shown in order to exclude the less reliable mechanisms obtained by analyses of the reported bulletin data alone. FMS were obtained by inversion of the first motion polarity readings from local and regional networks.

Considering Velebit and its hinterland (Lika Plateau) only, inspection of Fig. 9 reveals that most of the seismicity is related to Velebit itself, especially its southern part where epicenters closely follow the curvature of the mountain. Here the events are sharply confined to the area within the Velebit Fault system and the Lika backthrust. The earthquakes in the central part of Velebit, as well as in almost all of the Lika plateau are mostly weak, with only occasional occurrence of moderate events in central Lika. In these parts, seismicity is often related to several WNW–ESE striking reverse or strike-slip faults (e.g., the Bakovac Fault in Fig. 2). The eastern Lika Plateau, especially the greater area of the Bruvno dome, is currently practically aseismic. In the easternmost part of the investigated area shown in Fig. 9, earthquakes are related to a system of imbricated NNE-dipping reverse faults, possibly related to the Split-Karlovac Fault. In the NW-part of the studied area between Kvarner and Gorski

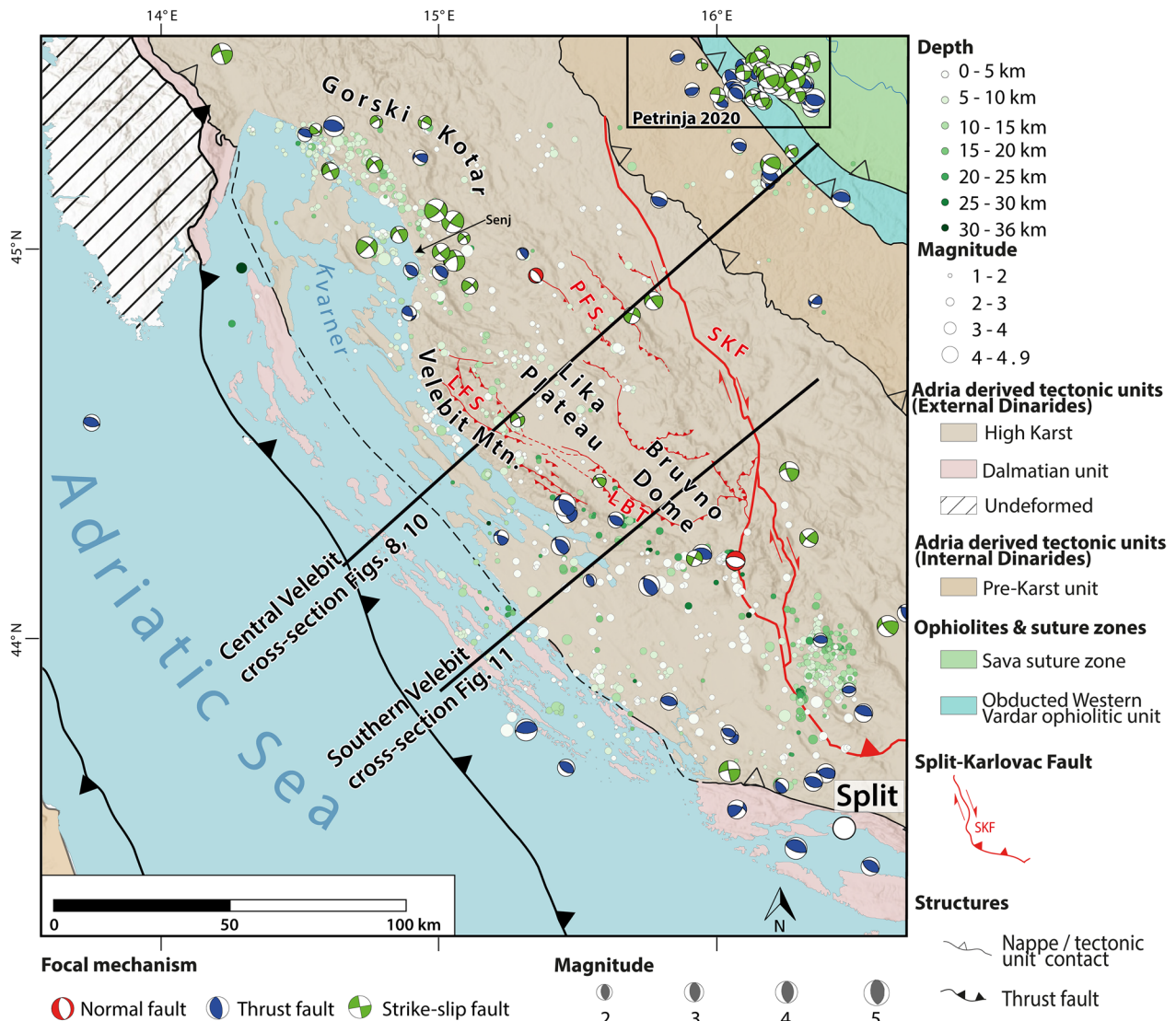


**Fig. 9** Tectonic units of a part of the northern External Dinarides after Schmid et al. (2020), supplemented by seismicity and focal mechanism solutions (FMS) for events occurred in the study area between 1995 and 2020 (Croatian Earthquake Catalogue, [CEC, Herak et al., 1996, updated until the end of 2020]). Only earthquakes with local magnitude  $M_L \geq 1.0$  and standard errors of the epicenter and focal depth of  $\sigma_E < 3$  km and  $\sigma_H < 4$  km, respectively, are shown. The magnitude is displayed by the symbol size, and the depth is color-coded (see the legend). The study area shows an overall low level of seismicity, with several areas of higher activity (e.g. the hanging wall of the Split-Karlovac Fault in the SE, and an active zone along the coast between Gorski Kotar and the Kvarner Gulf in the NW). Beneath Velebit seismicity is bimodal distributed. In the southern Velebit earthquakes are confined to its foreland, whereas the hinterland (Bruvno) is aseismic. This contrasts with the central Velebit, where earthquakes occur mostly in the hinterland. The FMSs show that the southern Velebit foreland is characterized by active thrusting, whereas the area between Kvarner and Gorski Kotar is related to predominantly strike-slip faulting

Kotar, earthquakes are more frequent and may exceed intensity VIII EMS (e.g. Herak et al., 2017, 2018; Palenik et al., 2019), which is also reflected in considerably higher level of seismic hazard there (Herak et al., 2011). They are mostly associated to a long, predominantly dextral strike-slip or transpressional Ilirska Bistrica–Senj active seismogenic zone (for details see Palenik et al., 2019).

Focal mechanisms in Fig. 9 are predominantly either reverse or strike-slip, with only a few normal faulting mechanisms associated with weak earthquakes. Analyses of the strike of the maximum horizontal local stress (P-axes) indicate its counterclockwise rotation from the (S)SW–(N)NE direction in the southern Velebit region to the predominant S–N orientation in the area northwest from Velebit.

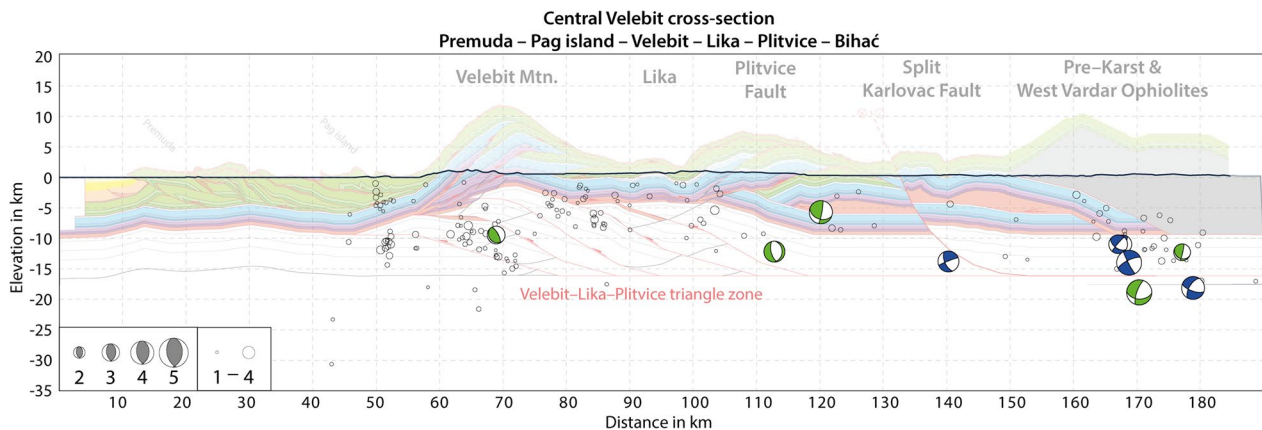


**Fig. 10** Seismicity of well localized events and the corresponding focal mechanisms (see Fig. 9) projected onto the central Velebit cross-section (Fig. 8) within a corridor of  $\pm 20$  km. The deeper seismic events cluster around the frontal tip of the Velebit-Lika-Plitvice triangle zone and the internal Pre-Karst High karst nappe contact. Shallow seismicity is recorded underneath the Lika Plateau and correlates with the modelled depth of the passive roof thrust. The focal mechanism solutions (FMS) are projected into the section plane; the colours correspond to the focal mechanisms in map view (Fig. 9). The FMS show that the frontal part of the section is mainly related to strike-slip faulting, whereas the internal part of the section is related to thrust faulting

## 6 Discussion

### 6.1 Seismicity

The projected seismicity within a 20 km wide swath shows a good overall correlation with the modelled structures in the Central Velebit cross-section (Fig. 10). In the Velebit foreland, most of the projected events are located at depths of 5–15 km and locally match the SW-vergent blind contractional duplexes underneath the Velebit Mtn. The more internal Lika Plateau is characterized by shallow seismicity, mostly above 5 km, which correlates with the depth of the modelled NE-vergent passive roof thrust. The deeper events, between 5 and 10 km depth, locally fit the blind duplexes underneath the Lika Plateau. The map view (Fig. 9) suggests the area around the Split-Karlovac Fault is aseismic, with only few events around this fault (Fig. 10). A cluster of seismic events is recorded around the Pre-Karst/High Karst nappe contact. Here most of the recorded earthquakes are located between 5 and 15 km depth.

Figure 9 shows that in vicinity to the Central Velebit cross-section only three FMS could be computed. All three indicate strike-slip faulting and were located between 5 and 12 km depth. The projection into the cross-section shows that the two most southern events correlate well with the blind duplexes, whereas the other event is located directly on the High Karst internal nappe stack (Fig. 10). The recorded FMS around the Pre-Karst/High Karst nappe contact in the northeast of the study area show primarily thrusting (Fig. 9). Projected into the Central Velebit cross-section, these events cluster here between 4 and 19 km depth (Fig. 10). The seismicity line up and form a c. 10 km wide active seismic zone.

Although the location and the dip of this seismic zone fits the modelled Pre-Karst/High Karst boundary in cross-section view, the deeper seismicity ( $>10$  km) does not correlate with the modelled flat in the cross-section and suggest a much deeper active fault (Fig. 10).

Figure 11 shows the Southern Velebit cross-section (Balling et al., 2021b) supplemented by projected seismic events within a swath of 20 km width. Most of the projected hypocentres are located within the frontal part of the cross-section, situated underneath Velebit and its foreland (Fig. 11). Directly under the Velebit Mtn. the recorded events cluster around 20 km depth and show a progressive shallowing towards the SW foreland. The projected data also show that the Velebit hinterland is aseismic; only two earthquakes are recorded around the Bruvno dome and no event was recorded around the Split-Karlovac Fault. Consequently, the FMS are only captured in the frontal part of the Southern Velebit cross-section, and they indicate mainly reverse faulting (Fig. 9). Projected into the section, this reveals that the frontal part of the Southern Velebit cross-section is dominated by deep (8–18 km depth) reverse faulting.

A comparison of both cross-sections with projected seismicity (Figs. 10, 11) shows that the instrumental seismicity along the Central Velebit cross-section correlates well with the modelled subsurface fault geometries (Fig. 8). Most earthquakes cluster around the frontal tip of the triangle zone and the Pre-Karst/High Karst nappe contact (Figs. 9, 10), suggesting that the Central Velebit triangle zone is taking up ongoing shortening. This is additionally supported by the



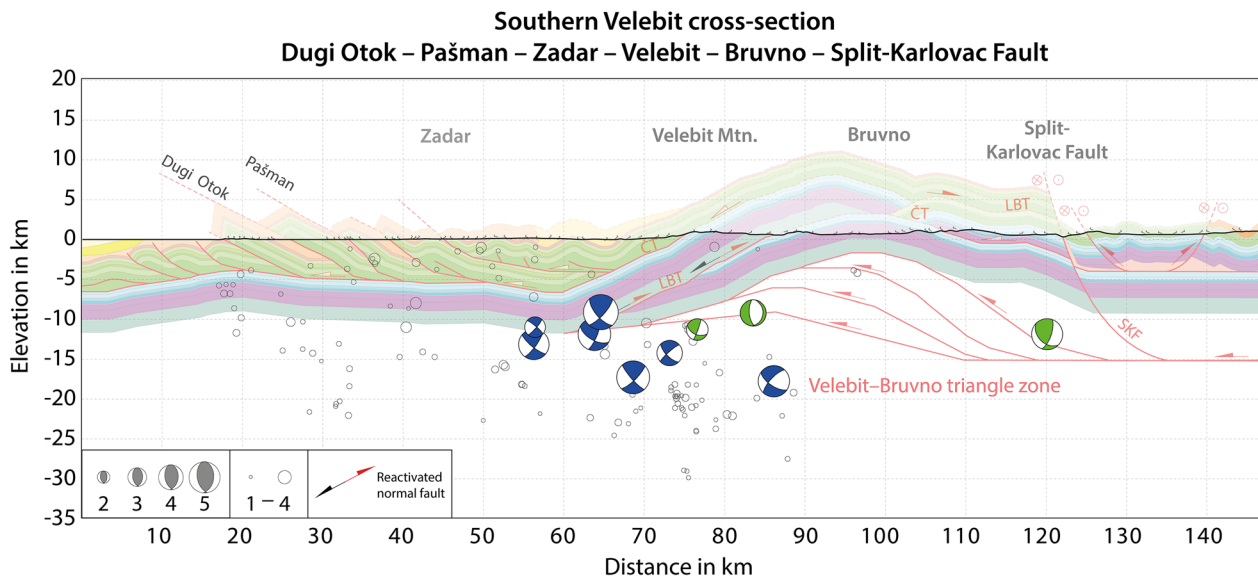


**Fig. 11** Seismicity of well localized events and corresponding focal mechanisms (see Fig. 9) projected onto the southern Velebit cross-section (modified after Balling et al., 2021b) within a corridor of  $\pm 20$  km. The section trace is displayed in Fig. 9. The projected seismicity shows poor correlation with structures modelled in the balanced cross-section. All recorded events are exclusively recorded within the southern Velebit foreland. The hinterland (Brvno) is aseismic. The focal mechanism solutions (FMS) are projected into the section plane, the colours correspond to the focal mechanisms in map view (Fig. 9). The FMS show that the southern Velebit foreland is characterized by deep (8–18 km) thrusting, suggesting an active outward propagation of basement thrusts at the base of the Velebit-Bruvno triangle zone towards SW

shallow seismicity captured underneath the Lika Plateau at the depth of the modelled NE vergent passive roof thrust detachment. Contrary to this, the modelled structures along the Southern Velebit cross-section do not correlate well with the projected seismicity (Fig. 11). In fact, the seismicity here suggests a thick-skinned and active outward propagation of the Southern Velebit triangle zone, shown by the deep reverse faulting and the accumulation of the seismicity exclusively in the frontal part of the cross-section.

Thus, the seismicity suggests that the Velebit-Bruvno triangle zone is actively outward propagating, whereas the central Velebit-Lika-Plitvice triangle zone is actively deforming internally (Figs. 9, 10, 11). This transition of the external vs. internal deformation corresponds with a number of backthrusts. In the central Velebit region the seismicity is distributed along the NE-vergent passive roof thrust toward the internal region and seems to be distributed along the five backthrusts of the Velebit and Plitvice Fault Systems (Fig. 8). However, in the case of the Southern Velebit cross-section, the seismicity is exclusively recorded in its foreland, while the internal Brvno region and the LBT are currently aseismic. This might indicate that the LBT and the Velebit-Bruvno triangle zone, or the deeper thick-skinned duplex, are currently locked, since not many events were registered here during the recorded timespan (Fig. 9).

Besides this rather local variation in seismicity also a more regional trend is captured by the seismic moment release map of the entire Dinarides (Ustaszewski et al., 2014, their Fig. 12). This map shows that the southern SW-nappe stack dominated External Dinarides are related to a 2–3 orders of magnitude higher seismic moment release in comparison to the northern NE-vergent backthrust dominated segment. Consequently it seems that the Eo-Oligocene backthrusts in the central Velebit cross-section (this study, Fig. 8) and the southern Velebit cross-section (Balling et al., 2021b; Fig. 11) are again acting as a backstop on the regional scale. This results in the comparatively low seismic moment release (Ustaszewski et al., 2014) and low seismicity levels across the greater Velebit area (Fig. 9). However, changes in the regional tectonic regime from Eo-Oligocene contraction to Miocene extension and finally a renewed Late Miocene change to contraction-transpressive deformation of the Dinarides have been postulated (Žibret & Vrabec, 2016; Andrić et al., 2017; van Unen et al., 2019).

## 6.2 Limits of the kinematic forward model

The best-fit final kinematic forward model of the Central Velebit cross-section (Fig. 8) correlates well with the recorded seismicity and portrays a thick-skinned triangle zone underneath the central Velebit Mountain. Within the Velebit-Lika-Plitvice triangle zone both Velebit Fault System and the Plitvice Fault System acted as a backstop

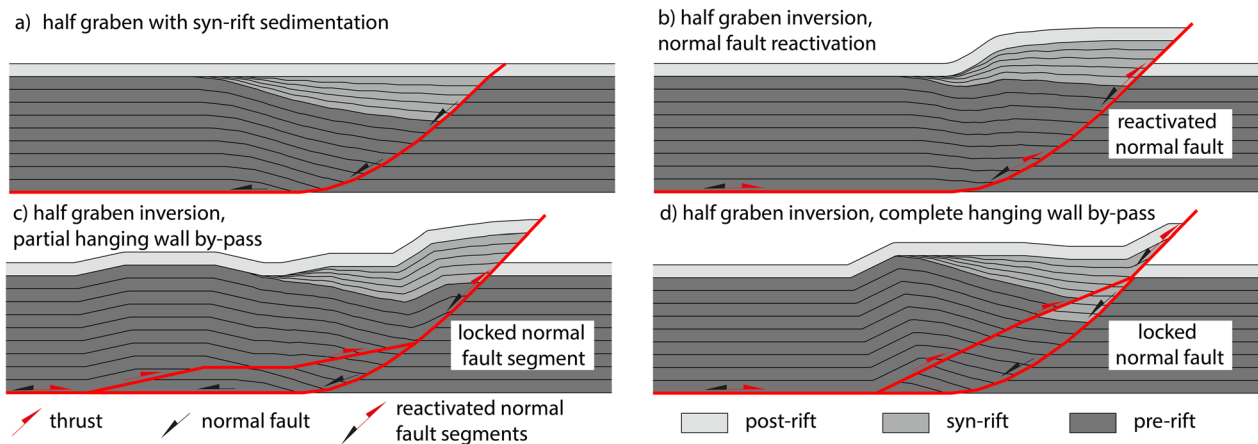


**Fig. 12** Schematic illustration of different inversions modes of a half graben, formed due to extension along a listric normal fault, containing pre-, syn- and post-rift sediments. **a** Half graben formation with roll-over anticline. **b** Complete reactivation of a normal fault, every normal fault segment is reactivated by reverse faulting, forming a harpoon/arrow-head anticline. **c** Shows a partial hanging wall by-pass, the lower part of the normal fault is locked and during shortening a new reverse fault geometry is formed, only the upper segment of the normal fault gets reactivated. **d** Complete hanging wall by-pass. In this basin inversion mode, the listric normal is not reactivated and the newly formed thrust ramps up into the post-rift sediments

(NE-vergent passive roof backthrusts) and prevented further propagation of the deformation towards the SW (Fig. 8). This is similar to the published 2D kinematic forward model of the Southern Velebit cross-section (Figs. 1d, 11; Balling et al., 2021b). Along this cross-section all of the shortening is accommodated along one backthrust, whereas in the Central Velebit cross-section shortening is accommodated by five backthrusts of the Velebit Fault System and the Plitvice Fault System (Figs. 6, 8). The width of the triangle zone differs in both models (Fig. 1a, e). In the Central Velebit cross-section the Velebit-Lika-Plitvice triangle zone is 75 km wide, whereas in the Southern Velebit cross-section the Velebit-Bruvno triangle zone is 65 km wide. The more tightly faulted and thick-skinned duplexes of the Velebit-Bruvno triangle zone led to the folding and uplift of the Bruvno dome (Figs. 2, 11). This must have also folded the backthrust in the Southern Velebit cross-section (Figs. 1d, 11; Balling et al., 2021b). This is in contrast to the Central Velebit cross-section, where the wider zone of compressional duplexes led to an uplifted and rather flat NE-vergent backthrust detachment and only gently folded Permian to Eocene strata of the Lika Plateau (Figs. 2, 8). The comparison of the two balanced kinematic models shows a similar amount of crustal shortening: along the Southern Velebit cross-section (Fig. 1e). Balling et al. (2021b) reported 89 km of shortening, while along the Central Velebit cross-section the amount of shortening is 94 km and 4 km of modelled Mesozoic extension (Fig. 8).

The described best-fit 2D kinematic forward model presents a plausible and consistent interpretation of the

subsurface structural architecture. However, the model relies on the balancing assumption, which requires that no material be moved in or out of the section plane. Consequently, the hanging wall movements along all faults, except for the Split-Karlovac Fault, were modelled to be deformed by plane strain. Due to the lack of reported thicknesses information on Triassic and older rock in the northeastern part of the cross-section, a constant thickness of the modelled units was assumed, despite of reported thickness variations of the Adriatic carbonate platform units (e.g. Tišljarić et al., 1998; Velić et al., 2002; Vlahović et al., 2005). A similar approach was followed to account for the Permian–Triassic rifting stage. Due to the lack of subsurface data in the northeastern part of the cross-section only the upper Middle Triassic (Ladinian,  $T_2^{2,3}$ ) and the Upper Jurassic (Lemeš unit,  $J_3^{2,3}$ ) successions were used as a marker horizon to quantify and model the passive margin extension (Fig. 4).

An exception to this balancing constraint is the thickness distribution of the Permian evaporites, located around the Split-Karlovac Fault between the Upper High Karst and Lower High Karst subunits (Fig. 8). Here lateral flow of evaporites into the plane of the section was assumed and all of the thin-skinned deformation is attributed to this lateral flow of evaporites. Due to the lack of seismic lines or borehole data in this region the shape and spatial distribution of the Permian evaporites around the Split-Karlovac Fault remains speculative. However, this assumption is supported by the official geological map sheet Bihać (Fig. 2; Polšak et al., 1976). A dome shape anticline with Middle Triassic carbonates

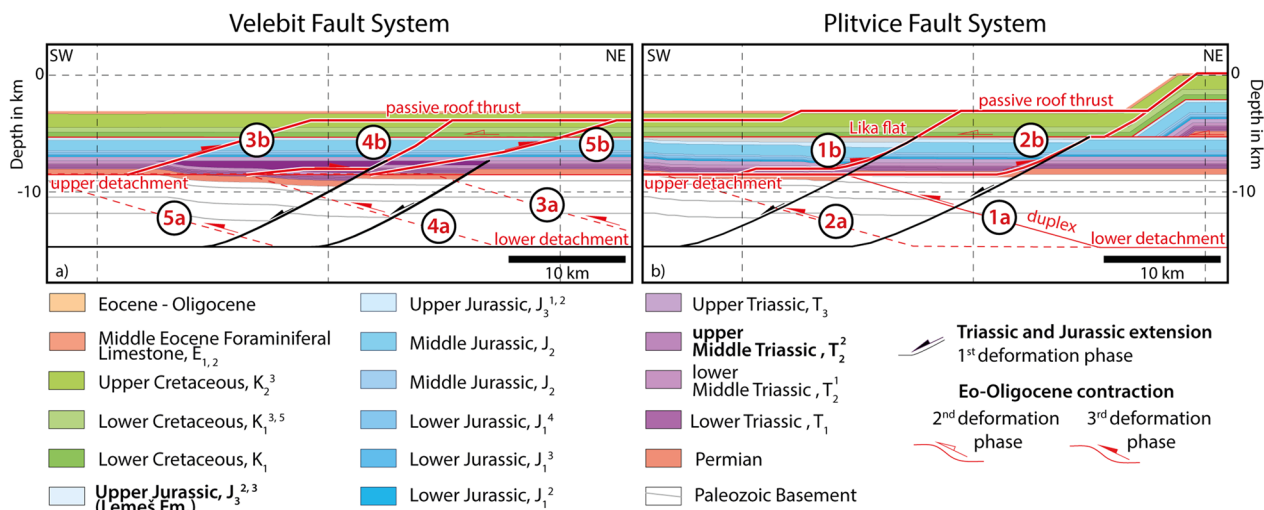


**Fig. 13** Modelled best-fit geometry of the Eo-Oligocene inversion of Mesozoic half graben systems. This figure is a zoom-in of the undeformed central part of the kinematic forward model (Fig. 6d) postdating deposition of the Middle Eocene Foraminiferal Limestone and formation of the High Karst internal nappe stack. The black lines represent normal faults generated during the Middle Triassic (a), (LTS) and Uppermost Jurassic (b), (PTS). The red faults show the modelled geometry of the generated backthrusts. The numbering of faults corresponds to the relative time of initiation of the faults. The blind duplex is marked by the letter 'a' and backthrusts are marked by the letter 'b'. **a** The reactivation of the LFS. Here the backthrusts 4 (Jadovno Fault) and 5 (Bužim Fault) by-passed the hanging wall of the two deep Middle Triassic normal faults, partly the normal fault geometry is reactivated. Backthrust 3 (Brušane-Oštarije Fault) is not related to a previous normal fault, since no Middle Triassic was deposited within the hanging wall (Fig. 3a). **b** The inversion of the Plitvice Fault System. Here the best-fit geometry suggests that the normal faulting occurred during upper Jurassic and that the half grabens were inverted during the Cenozoic contraction mainly by hanging wall by-passes

exposed in its core is located north of the city of Bihać. In order to explain this map pattern and to keep the assessed crustal shortening minimal we attributed this to lateral flow of subsurface Permian evaporites. Modelling the viscous lateral flow of evaporites requires fault unrelated folding. This marks one of the limitations of the balanced cross-section technique and consequently also 2D kinematic forward modelling methods. An assumed fully brittle deformation for this area would have added 5–10 km additional crustal shortening to our results.

### 6.3 Inversion of Mesozoic graben structures

Throughout the iterative 2D kinematic forward modelling approach, a variety of deformation scenarios, fault geometries and detachment depths were tested. The best-fit kinematic model suggests an inversion of Mesozoic basement-rooted normal faults during the Eo-Oligocene contractional deformation. Figure 12 schematically illustrates a variety of basin inversion modes applied in this study. A roll-over anticline is formed above a listric fault geometry (Fig. 12a). This basin is inverted either by the complete reactivation of the normal fault (Fig. 12b), or by hanging wall by-passes (Fig. 12c, d). During a partial reactivation of a hanging wall by-pass only the upper normal fault segment is inverted, while the lower segment of the normal fault is locked, and normal fault segments are by-passed by a newly formed reverse fault

geometry (Fig. 12c). During a complete hanging wall by-pass inversion of a half graben no segment of the normal fault is inverted. Shortening is accommodated along a newly formed reverse/thrust fault by-passing the listric normal fault geometry (Fig. 12d).

Figure 13a shows the best-fit modelled fault geometries for the Velebit Fault System, illustrating that two deep Middle Triassic half grabens were inverted by two Eo-Oligocene backthrusts. The normal faults are rooted in the basement at a depth of about 15 km, whereas the backthrust roots into the future passive roof thrust detachment at the base of the Permian. The best-fitting fault geometry for backthrust #4b (Fig. 13) portrays a partial hanging wall by-pass, in which only the upper part of the Triassic normal fault above the upper detachment got inverted. The best-fit geometry for backthrust #5b (Fig. 13) suggests a complete hanging wall by-pass, since no part of the Triassic normal fault got inverted. Although backthrust #3b did not invert an extensional basin, our model suggests that this fault was initiated at the Middle Triassic syn-rift facies transition (Fig. 13a). The final modelled deformed section (Fig. 8) fits the map pattern (Fig. 2) and explains the facies transition across the backthrusts in the Velebit Fault System (Figs. 4a, 6a). Additionally, it accounts for the formation of deep Middle Triassic half grabens



(Lawrence et al., 1995; Smirčić et al., 2020) caused by the break-up of Adria (Pamić, 1984).

Figure 13b shows the layer cake model and the best-fit modelled fault geometries for the Plitvice Fault System prior to contractional deformation. It illustrates that here the late Jurassic normal faults led to the local deposition of the Lemeš unit. The modelled geometry for the two latest Jurassic normal faults is similar to the geometry used for the Middle Triassic extension (Fig. 13a). It shows two deep-seated Jurassic normal faults, which became inverted by Eo-Oligocene backthrusts. The modelled backthrust #1b has a flat-ramp geometry; the upper part of the Jurassic normal fault is used as the last ramp segment for the backthrust #1b. Backthrust #2b inverts half of the adjacent Jurassic normal fault and ramps up into the frontal limb of the High Karst internal nappe stack (Fig. 13b). Both normal faults root at 15 km depth, at the same depth as for the detachment of the blind duplexes. The final kinematic forward model (Fig. 8) indicates that the Plitvice Fault System deformed before the Velebit Fault System.

In addition to the Middle Triassic normal faults that were inverted as backthrusts of the Velebit Fault System, we presumed that the deposition of the Lemeš unit was also related to local normal faulting during latest Jurassic times (Fig. 13b), as supposed by Bucković et al. (2004). However, the tectonic regime during the deposition of the deep-water Lemeš unit in Late Jurassic times is still debated. Various models consider the obduction of the ophiolites in the Internal Dinarides as the cause of opening of the Latest Jurassic Lemeš Basin. One model considered the Late Jurassic opening of a pull apart basin in the Adriatic carbonate platform due to transferred contraction related to the obduction in the Internal Dinarides (Velić et al., 2002; Bucković & Markić, 2016; Vlahović et al., 2005). Another model suggests that obduction-related contractional far-field effects led to buckling of the lithosphere, explaining the Late Jurassic subsidence in part of the Adriatic carbonate platform, similarly to paleoenvironmental changes reported from the Belluno Basin in northern Italy (Picotti & Cobianchi, 2017). Based on a detailed lithostratigraphic study and the lack of mass transport deposits within the Lemeš unit, the lithosphere buckling model was also adapted for the deposition of the Lemeš unit in the External Dinarides (Vitzthum et al., 2022). Due to the lack of sedimentary evidence for normal faulting, Vitzthum et al. (2022) rejected a possible extension-related Late Jurassic basin formation.

In our regional-scale kinematic forward model we proposed that normal faults were the most plausible and geometrically viable solution for the subsidence of the Lemeš Basin. The tectonic load of the obducted ophiolites in the Internal Dinarides could lead to flexure of the

lithosphere, as also observed in the India-Asia collision (Beck et al., 1996). This regional flexure could have led to either local formation of new Upper Jurassic normal faults or to the reactivations of inherited Middle Triassic half grabens (Figs. 3, 4a). Due to the lack of exposures older than Upper Triassic and subsurface data from the Plitvice Fault System, a possible reactivation of Middle Triassic normal faults in Late Jurassic time is speculative. Nevertheless, the kinematic forward model presented in Fig. 8 shows that similar normal fault geometries assumed for both the Middle Triassic and Late Jurassic extension leads to a balanced cross-section, representing the present-day deformed state (Fig. 8).

The inversion of an extensional basin implies that the basin infill was exhumed or uplifted due to reversal of subsidence by contractional tectonics (Lake & Karner, 1987; Williams et al., 1989; Zwaan et al., 2022). This reversal may occur with or without the inversion of normal faults. The Central Velebit cross-section (Fig. 8) proposes that the study area experienced a minimal Mesozoic extension of 4 km and an Eo-Oligocene shortening of 94 km. A review of analogue models reveals that the style of inversion depends on initial basin geometry, brittle vs. ductile deformation, the angle of inversion indentation (oblique/orthogonal inversion), the geometry and mechanical properties of the basin filling, and the shortening rate (Zwaan et al., 2022).

The amount of different parameters controlling the geometry and style of inversion leads to a variety of reported inversion geometries. A field study from the northwestern Alpine foreland shows that a Miocene triangle zone developed on top of an inverted normal fault (Malz et al., 2016). Based on seismic data, Malz et al. (2016) showed that a triangle zone used multiple secondary (upper) detachments in various Mesozoic strata and inverted a part of four adjacent normal faults. Another case study showing the inversion tectonics resulting in a triangle zone offshore New Zealand is presented in Barnes and Nicol (2004). They showed the Miocene to recent inversion of the 44 km long normal fault, which is located on top of a thrust duplex. The interpreted seismic lines show that the extensional basin is inverted by the small-scale backthrust, rooting into the former normal fault detachment (Barnes & Nicol, 2004).

None of the reported triangle geometries is in line with our results from the kinematic forward model. The modelled inversion of the Velebit Fault System shows hanging wall by-pass backthrust geometries (Fig. 13a). According to numerical modelling such hanging wall by-passes are favoured by the presences of weak syn-rift sediments (Granado & Ruh, 2019). The same study states that an upper detachment fundamentally controls the structural style of inversion and favours the inversion of syn-rift

**Table 1** Summary of the reported mechanical, rheological and erosional factors controlling formation of a triangle zone (passive roof thrust duplex). The table shows how individual parameters favour either the initiation of an active or a passive roof thrust. These factors are compared to the External Dinarides fold-and-thrust belt

Parameter	Active roof thrust	Passive roof thrust	Likelihood	Details of regional geological setting
Heterogeneities in the mechanical stratigraphy (Couzens-Schultz et al., 2003; Couzens & Wiltchko, 1996)	Low	High	High	Mainly carbonates in the overburden low grade metamorphic shales in the Paleozoic, no data from the southern External Dinarides
Upper detachment (Costa & Vendeville, 2002; Couzens-Schultz et al., 2003; Dean et al., 2013; Jamison, 1996)	Weak	Strong	High	Mechanical difference east and west of the Split-Karlovac Fault likely favoured the along-strike contrasting style of deformation
Influence of pre-existing structure/Lateral facies changes (Albanese & Sulli, 2012; Erickson, 1995; Malz et al., 2016; Mohn et al., 2014)	Low	High	High	Middle Triassic half graben (Lawrence et al., 1995; Smirčić et al., 2020), Lemeš Basin (Velić et al., 2002; Vitzthum et al., 2022)
(tectonic) Overburden (Bonini, 2001, 2003; Jamison, 1996)	Low	High	Possible	Pre-triangle zone crustal thickening, due to nappe stack
Differential Erosion & Syn-tectonic deposits (Erdős et al., 2015; Fillon et al., 2013; Mugnier et al., 1997)	Low	High	Low	No erosion data, but high erosion within the Velebit Mtn., no syn-tectonic deposits in the frontal Velebit part
Shortening rate (Couzens-Schultz et al., 2003)	Low	High	Excluded	No data; excluded, higher amount of shortening in the active roof thrust segment (Balling et al., 2021b)
Buttress (backstop) (Albanese & Sulli, 2012; Couzens-Schultz et al., 2003; Erickson, 1995; Jamison, 1996)	No	Yes	Excluded	Not known in the Adriatic Sea and considered unlikely

basins (Granado & Ruh, 2019). In addition to this, our results indicate that the thick-skinned Mesozoic normal faults were reactivated by shallower thrust, rooted with the upper part of the Carboniferous (Adriatic basement, Fig. 13). A similar style of inversion tectonics is reported by Scisciani (2009) who showed that pre-existing mainly Jurassic normal faults controlled the localization, spacing and kinematics of the propagating thin-skinned thrust ramps in the central Apennines.

#### 6.4 Mechanical properties favouring the formation of triangle zones

In the past decades mechanical properties controlling the initiation and formation of triangle zones with passive roof thrusts were determined by analogue and numerical models (Table 1). Such models show that the presence of a weak upper detachment favours the initiation of active roof thrusts, whereas a strong upper detachment leads to the initiation of passive roof thrusts/triangle zones (Banks & Warburton, 1986; Jamison, 1996; Costa & Vendeville, 2002; Bonini, 2003; Couzens-Schultz et al., 2003). Due to the lack of evaporites in the upper (passive roof thrust) detachment of the Velebit triangle zones the upper detachment is rather strong west of the Split-Karlovac Fault, favouring the formation of passive roof thrusts. In contrast, Fig. 4 shows that the eastern sector of this fault is characterized by the presence of Permian evaporites. Balling et al. (2021b) demonstrated that the top of these evaporites was used as the main detachment

during Eo-Oligocene folding and thrusting in this part of the External Dinarides. This led to a contrasting style of deformation east of the Split-Karlovac Fault, characterized by SW-vergent outward propagation of faults along mechanically weak evaporitic detachment, favouring the formation of active roof thrust (Fig. 1e). Consequently, the mechanical difference of detachment east and west of the Split-Karlovac Fault likely favoured the along-strike contrasting style of deformation of the External Dinarides.

Another factor controlling the formation of triangle zones is a high shortening rate, which increases the mechanic coupling between the overburden and the underlying duplex across viscous detachments (Ustaszewski et al., 2005), promoting the formation of backthrusts (Couzens-Schultz et al., 2003). An along-strike variation of the shortening rates can be excluded in our case, because flexural subsidence modelling showed that areas of contrasting style of structural architecture deformed contemporaneously (Balling et al., 2021b).

Most triangle zones, situated in the frontal part of fold-and-thrust belts, formed due to the presence of a buttress or backstop (Erickson, 1995; Jamison, 1996; Couzens-Schultz et al., 2003; Albanese & Sulli, 2012). Such backstops prevent further propagation of the deformation towards more external parts and lead to large-scale underthrusting (Couzens-Schultz et al., 2003). Albanese and Sulli (2012) showed that an African paleo-margin offshore west of Sicily acted as a backstop and initiated the formation of a Miocene triangle zone. There are no

reports of such a paleo-topographic features within our study area, neither offshore nor onshore. Consequently, the presence of a pre-deformational Eo-Oligocene backstop seems unrealistic in our case.

Mugnier et al. (1997) studied the influence of the interplay of erosion and syn-tectonic deposition in a sandbox model and showed that restrained erosion also leads to the development of major backthrusts. Other numerical models of the deformation of a thin-skinned orogen show that an increase in syn-tectonic sedimentation can initiate local backthrusts (Fillon et al., 2013). There are no available quantitative data from the External Dinarides neither about the erosional nor syn-orogenic depositional rates during Eo-Oligocene times. However, the Basic Geological Map sheets Gospić (Sokač et al., 1974), Udbina (Šušnjar et al., 1973) and Obrovac (Ivanović et al., 1973) and the Southern (Figs. 1e, 11) and Central Velebit (Figs. 1d, 8, 10) cross-sections suggest that the total amount of erosion must have been high within the study area, exposing the Paleozoic basement in this area (Fig. 2). Additionally, the total amount of preserved Eo-Oligocene syn-tectonic deposits is highly variable along-strike of the External Dinarides. In the southeastern foreland of the Velebit Mtn. an up to 2 km thick sequence of Eo-Oligocene Promina Beds is exposed (Fig. 2), whereas in the NW only a condensed up to 30 m thick sequence of contemporaneous deposits is preserved (Babić et al., 1993). Balling et al. (2021b) showed that the Promina Beds were deposited contemporaneously with the folding and thrusting of the Velebit triangle zones. Based on thermomechanical models, Erdős et al. (2015) demonstrated that a foreland of a sediment-starved orogenic systems is generally characterized by thin-skinned deformation, whereas a foreland of the sediment-loaded orogen is characterized by thick-skinned deformation. This might indicate that the syn-tectonic sedimentary load of the Promina Beds additionally contributed to the development of the thick-skinned triangle zone.

An additional factor controlling the initiation of backthrust is the thickness of the overburden. Sandbox models show that active roof thrusts are initiated when the thickness of the overlying brittle layer is up to double of that of the underlying viscous layer (Bonini, 2001, 2003). If the thickness of the brittle layer exceeds 2.5 times the thickness of the viscous lower layer, passive roof thrusts are initiated (Bonini, 2001, 2003). In other words, folding and thrusting prior to the formation of the triangle zone could have led to a thicker overburden, which in turn would favour the formation of backthrusts and deep blind duplexes. The kinematic evolution of the central Velebit Mtn. Figure 8b–e shows that during the first contractional deformation phase the thin-skinned deformation was shifted towards the SW into the most external

part of the studied section along the 80 km long Lika flat that served as a detachment at the base of the Cretaceous (Fig. 8d). Although large parts of the Cretaceous and Eocene units are eroded in the Velebit Mtn., there is no substantial evidence for pre-triangle zone crustal thickening due to thrusting within the Lika Plateau area, because the Upper and Lower Cretaceous units are not fault bounded here (Figs. 2, 8).

### 6.5 Along strike variations in the mechanical stratigraphy

Based on (i) the comparison of the along-strike variations in the lithostratigraphy and the resulting detachment geometries/depth (Fig. 14) and (ii) based on the mechanical factors controlling the formation of triangle zones (Table 1), we propose that the most plausible cause for the initiation of the triangle structure in Velebit Mtn. and deformation in its hinterland is caused by lateral facies changes within the Permian sedimentary succession (Figs. 3, 4, 14). The lack of Permian evaporites in the Velebit Mtn. led to the establishment of a stronger upper detachment in the upper part of the Palaeozoic basement during the Eo-Oligocene folding and thrusting (Fig. 14). Such a strong upper detachment favours the formation of triangle zones (Jamison, 1996; Costa & Vendeville, 2002; Couzens-Schultz et al., 2003; Dean et al., 2013). An additional factor favouring this style of deformation is the inversion of the Mesozoic half grabens (Fig. 8; Additional file 2). These inherited faults and the related Mesozoic syn-rift sediments acted as zones of contrasting mechanical weaknesses, serving as a nucleus for the backthrusts (Fig. 13). In contrast, the Permian evaporites along the Split cross-section, east of the Split-Karlovac Fault (Figs. 2, 3, 4, 13), served as a weak basal detachment (Figs. 1e, 2). This led to an in-sequence deformation along an up-stepping detachment.

Yet another difference in the style of deformation between the Split cross-section and the Central Velebit cross-section is the 80 km long Lika flat found in the latter (Fig. 8). This flat developed during the first deformational step related to the High Karst nappe, detaching the Lower Cretaceous from the underlying strata. Along this detachment the thin-skinned deformation was transferred into the Velebit foreland, pre-dating the formation of the triangle zone (Fig. 8d). Deep boreholes from Velebit foreland (Figs. 2, 4) show that anhydrite is present at this stratigraphic level. Most likely this mechanical weak layer was used as a detachment, leading to higher tectonic load or overburden in the Velebit foreland (Fig. 8d). This foreland tectonic load might have additionally contributed to the formation of the Velebit triangle zone.

Although a High Karst-internal nappe stack is also observed along the Split cross-section this internal nappe stack was not related to the formation of a long



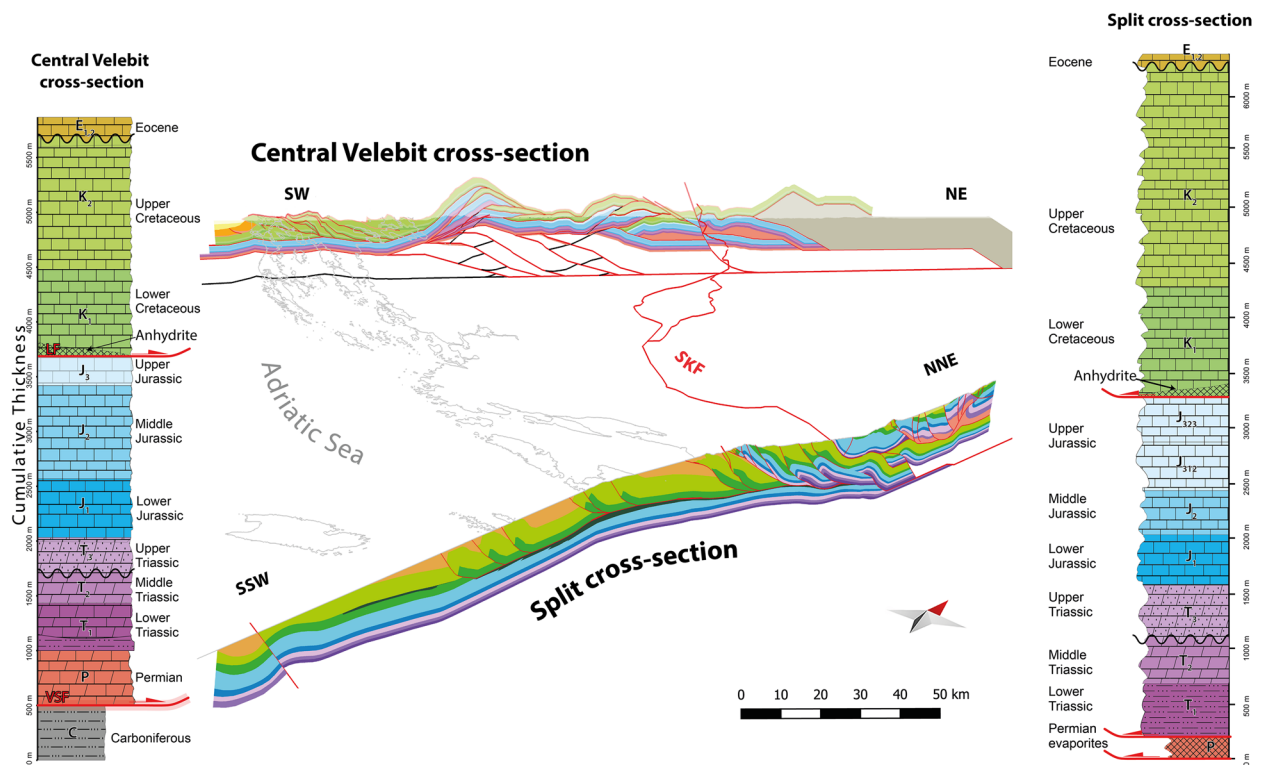


**Fig. 14** 3D view of the study area showing the Central Velebit cross-section (this study) in the NW and the Split cross-section (Balling et al., 2021b) in the SE. The coastline and the fault trace of the Split-Karlovac Fault is displayed in between. The lithostratigraphic log on the left shows the compiled thicknesses and main detachment horizons for the Central Velebit cross-section, whereas the lithostratigraphic log shows similar information for the Split cross-section

flat detachment at the base of Cretaceous strata (Fig. 14). Consequently no thin-skinned shortening was transferred along such flat into the foreland. The Split cross-section portrays an in-sequence style of deformation, although the Lower Cretaceous anhydrite-dolomite complex is also present in the southwestern foreland along the Split cross-section (Fig. 14). Here, this complex served as a detachment only during the latest stages of folding and thrusting of the most external part (Fig. 14).

## 7 Conclusion

The presented 2D kinematic forward model of the Central Velebit cross-section shows that the Eo-Oligocene deformation was related to the formation of a complex Velebit-Lika-Plitvice triangle zone in this part of the External Dinarides. This 75 km wide triangle zone consists of five NE-vergent thin-skinned backthrusts detached along Upper Paleozoic siliciclastic rocks located between 10 and 4 km depth and above the thick-skinned, SW-vergent system of blind thrust duplexes formed in a depth of 15 km in the underlying Adriatic basement. The balanced cross-section across the Central Velebit Mtn. yields a minimal crustal shortening of 94 km, similar

to the shortening of 89 km across the Southern Velebit cross-section.

Based on considerations of the mechanical stratigraphy, altered by the presence of inherited Mesozoic half grabens and the 2D kinematic forward model, we extracted the three most plausible factors that led to the observed along-strike contrasts in Eo-Oligocene deformation styles of the central External Dinarides, including the formation of the Velebit triangle zone:

1. The along-strike facies transition of the Permo-Triassic evaporites: East of the Split-Karlovac Fault the top of these evaporites served as a thin, weak detachment, favouring a SW-vergent outward nappe propagation that resulted in 113 km of Eo-Oligocene shortening along the Split cross-section (Fig. 1e). However, to the west of the Split-Karlovac Fault the lack of evaporites led to the displacement of the Adriatic carbonate sequence along the upper part of the Adriatic basement. This thicker but stronger detachment favoured the initiation of a thick-skinned triangle zone.

2. The inversion of Mesozoic half grabens: Our results show that all backthrusts nucleated at the rims of either Middle Triassic or Upper Jurassic half grabens. Although these Mesozoic normal faults were only partly inverted, our results suggest that the related syn-rift sediments have altered the mechanical stratigraphy and acted as locations for strain nucleation during the Cenozoic shortening phase. This led to the best-fit hinterland propagating backthrusts, contrary to theoretical models of triangle zone formation, which favour a foreland propagating backthrust system.
3. The presence of anhydrite at the base of the Lower Cretaceous: Anhydrite additionally facilitated the along-strike changes in structural style.

The distribution of instrumentally recorded seismicity shows that the Velebit triangle zones is related to a considerably weaker seismic moment release compared to the rest of the External Dinarides. Earthquake hypocentres show a good correlation with the kinematically forward modelled subsurface faults along the Central Velebit cross-section. Despite the reported Neogene change in the regional tectonic regime of the Dinarides, the seismicity captured in the Velebit-Lika-Plitvice triangle zone suggests renewed or ongoing shortening in both structural levels. This shortening seems to be distributed along the deeper blind duplexes and along the shallower passive roof thrust. This contrasts with the southerly adjacent southern Velebit cross-section, where seismicity is restricted to the southern Velebit foreland. The Velebit-Bruvno triangle zone itself is aseismic, but shows evidence of active outward propagation of the deformation. Our results demonstrate that lateral heterogeneities, caused by sedimentary variation or by the reactivation of older faults, within the mechanical stratigraphy not only exert control over the style of Cenozoic folding and thrusting, but also over the distribution of the seismicity in the External Dinarides.

## Supplementary Information

The online version contains supplementary material available at <https://doi.org/10.1186/s00015-023-00437-0>.

**Additional file 1.** Used modelling parameters and used kinematic algorithms for the best-fit 2D kinematic forward model.

**Additional file 2.** Animation of the deformation of the Central Velebit cross-section. This animation is based on 30 original frames. Additional frames were interpolated to increase the smoothness of the animation by the usage of the software DAIN.

## Acknowledgements

We thank two anonymous reviewers and A. Malz for their very constructive comments and helpful remarks, which greatly helped to further improve our

manuscript. We acknowledge Stefan M. Schmid for additional comments and dedicated editorial work. We also acknowledge developers and contributors of the General Mapping Tool (GMT), which was used to prepare several figures in this manuscript. Furthermore, we acknowledge the DEAL Project for founding this Open Access publication.

## Author contributions

PB, BT and KU conducted fieldwork in the External Dinarides. PB kinematically modelled the balanced cross-section. MH relocated the earthquakes. MH and PB jointly performed the seismotectonic analysis. All authors contributed to discussing and interpreting their results and jointly wrote the final manuscript.

## Funding

Open Access funding enabled and organized by Projekt DEAL.

## Availability of data and materials

Not applicable.

## Declarations

## Ethics approval and consent to participate

Not applicable.

## Consent for publication

Not applicable.

## Competing interests

The authors declare no conflict of interest.

## Author details

<sup>1</sup>Institute for Geological Sciences, Friedrich-Schiller-Universität Jena, Burgweg 11, 07749 Jena, Germany. <sup>2</sup>Faculty of Mining, Geology & Petrol Engineering, University of Zagreb, Pierottijeva 6, 10000 Zagreb, Croatia. <sup>3</sup>Faculty of Science, University of Zagreb, Horvatovac 102a, 10000 Zagreb, Croatia.

Received: 6 September 2022 Accepted: 29 May 2023

Published online: 21 June 2023

## References

- Albanese, C., & Sulli, A. (2012). Backthrusts and passive roof duplexes in fold-and-thrust belts: The case of Central-Western Sicily based on seismic reflection data. *Tectonophysics*, 514, 180–198.
- Aljinović, D., et al. (2018). Western Tethyan epeiric ramp setting in the Early Triassic: An example from the Central Dinarides (Croatia). *Journal of Earth Science*, 29(4), 806–823.
- Amoco. (1990). *Preliminary structural evaluation of the Croatian Dinarides regional structural cross section montage*. Amoco Yugoslavian Petroleum Company.
- Andrić, N., et al. (2017). The link between tectonics and sedimentation in asymmetric extensional basins: Inferences from the study of the Sarajevo-Zenica Basin. *Marine and Petroleum Geology*, 83, 305–332.
- Babić, L., Zupanić, J., & Crnjaković, M. (1993). An association of marine tractive and gravity flow sandy deposits in the Eocene of the NW part of the Island of Pag (Outer Dinarides, Croatia). *Geologia Croatica*, 46(1), 107–123.
- Bagagli, M., Molinari, I., Diehl, T., Kissling, E., & Giardini, D. (2022). The AlpArray research seismicity-catalogue. *Geophysical Journal International*, 231(2), 921–943.
- Bahun, S. (1974). The tectogenesis of Mt. Velebit and the formation of Jelar-deposits. *Geološki Vjesnik*, 27, 35–51.
- Balling, P., Grützner, C., Tomljenović, B., Spakman, W., & Ustaszewski, K. (2021a). Post-collisional mantle delamination in the Dinarides implied from staircases of Oligo-Miocene uplifted marine terraces. *Scientific Reports*, 11(1), 2685.
- Balling, P., Tomljenović, B., Schmid, S. M., & Ustaszewski, K. (2021b). Contrasting along-strike deformation styles in the central external Dinarides assessed by balanced cross-sections: Implications for the tectonic

- evolution of its Paleogene flexural foreland basin system. *Global and Planetary Change*, 205, 103587.
- Banks, C., & Warburton, J. (1986). 'Passive-roof' duplex geometry in the frontal structures of the Kirthar and Sulaiman mountain belts, Pakistan. *Journal of Structural Geology*, 8(3–4), 229–237.
- Bao, W., et al. (2019). Depth-aware video frame interpolation. In Proceedings of the IEEE/CVF conference on computer vision and pattern recognition (pp. 3703–3712).
- Barnes, P. M., & Nicol, A. (2004). Formation of an active thrust triangle zone associated with structural inversion in a subduction setting, eastern New Zealand. *Tectonics*. <https://doi.org/10.1029/2002TC001449>
- Beck, R. A., Burbank, D. W., Sercombe, W. J., Khan, A. M., & Lawrence, R. D. (1996). Late Cretaceous ophiolite obduction and Paleocene India-Asia collision in the westernmost Himalaya. *Geodinamica Acta*, 9(2–3), 114–144.
- Bonini, M. (2001). Passive roof thrusting and forelandward fold propagation in scaled brittle-ductile physical models of thrust wedges. *Journal of Geophysical Research: Solid Earth*, 106(B2), 2291–2311.
- Bonini, M. (2003). Detachment folding, fold amplification, and diapirism in thrust wedge experiments. *Tectonics*. <https://doi.org/10.1029/2002TC001458>
- Boyer, S. E., & Elliott, D. (1982). Thrust systems. *Aapg Bulletin*, 66(9), 1196–1230.
- Bucković, D., & Markić, A. (2016). Correlation of carbonate strata in Gorski Kotar Area (Karst Dinarides, Croatia), An example of adriatic carbonate platform environmental diversity during the Late Jurassic. *International Journal of Earth & Environmental Sciences*, 1, 1–9.
- Bucković, D., Tešović, B. C., & Gušić, I. (2004). Late Jurassic paleoenvironmental evolution of the western Dinarides (Croatia). *Geologica Carpathica*, 55(1), 3–18.
- Buiter, S. J., Pfiffner, O. A., & Beaumont, C. (2009). Inversion of extensional sedimentary basins: A numerical evaluation of the localisation of shortening. *Earth and Planetary Science Letters*, 288(3–4), 492–504.
- Bulić, J., & Jurišić-Poljak, Z. (2009). Macropalaeontology and stratigraphy of lacustrine Miocene deposits at Crnika beach on the Island of Pag (Croatia). *Geologia Croatica*. <https://doi.org/10.4154/GC.2009.16>
- Butler, R. W., Tavarneri, E., & Grasso, M. (2006). Structural inheritance in mountain belts: An Alpine-Apennine perspective. *Journal of Structural Geology*, 28(11), 1893–1908.
- Casas-Sainz, A. M., & Simón-Gómez, J. (1992). Stress field and thrust kinematics: A model for the tectonic inversion of the Cameros Massif (Spain). *Journal of Structural Geology*, 14(5), 521–530.
- Cawood, A. J., & Bond, C. E. (2018). 3D mechanical stratigraphy of a deformed multi-layer: Linking sedimentary architecture and strain partitioning. *Journal of Structural Geology*, 106, 54–69.
- Chorowicz, J. (1975). Mechanics of Split-Karlovac transversal structure in Yugoslavian Dinarides. *Comptes rendus hebdomadaires des séances de l'Académie des sciences*, 280(20), 2313–2316.
- Cooke, M., Mollema, P., Pollard, D., & Aydin, A. (1999). Interlayer slip and joint localization in the East Kaibab Monocline, Utah: Field evidence and results from numerical modelling. *Geological Society, London, Special Publications*, 169(1), 23–49.
- Corbett, K., Friedman, M., & Spang, J. (1987). Fracture development and mechanical stratigraphy of Austin Chalk, Texas. *AAPG Bulletin*, 71(1), 17–28.
- Ćosović, V., Mrinjek, E., Nemec, W., Španiček, J., & Terzić, K. (2018). Development of transient carbonate ramps in an evolving foreland basin. *Basin Research*, 30(4), 746–765.
- Costa, E., & Vendeville, B. (2002). Experimental insights on the geometry and kinematics of fold-and-thrust belts above weak, viscous evaporitic décollement. *Journal of Structural Geology*, 24(11), 1729–1739.
- Couzens, B. A., & Wiltzschko, D. V. (1996). The control of mechanical stratigraphy on the formation of triangle zones. *Bulletin of Canadian Petroleum Geology*, 44(2), 165–179.
- Couzens-Schultz, B. A., Vendeville, B. C., & Wiltzschko, D. V. (2003). Duplex style and triangle zone formation: Insights from physical modeling. *Journal of Structural Geology*, 25(10), 1623–1644.
- Coward, M. P. (1996). Balancing sections through inverted basins. *Geological Society, London, Special Publications*, 99(1), 51–77.
- Coward, M., Gillcrist, R., & Trudgill, B. (1991). Extensional structures and their tectonic inversion in the Western Alps. *Geological Society, London, Special Publications*, 56(1), 93–112.
- Dahlen, F. (1990). Critical taper model of fold-and-thrust belts and accretionary wedges. *Annual Review of Earth and Planetary Sciences*, 18, 55.
- Dahlstrom, C. D. (1970). Structural geology in the eastern margin of the Canadian Rocky Mountains. *Bulletin of Canadian Petroleum Geology*, 18(3), 332–406.
- Davies, V. M. (1982). Interaction of thrusts and basement faults in the French external Alps. *Tectonophysics*, 88(3–4), 325–331.
- Davis, D., Suppe, J., & Dahlen, F. (1983). Mechanics of fold-and-thrust belts and accretionary wedges. *Journal of Geophysical Research: Solid Earth*, 88(B2), 1153–1172.
- De Graciansky, P., Dardeau, G., Lemoine, M., & Tricart, P. (1989). The inverted margin of the French Alps and foreland basin inversion. *Geological Society, London, Special Publications*, 44(1), 87–104.
- de Leeuw, A., Mandic, O., Krijgsman, W., Kuiper, K., & Hrvatović, H. (2012). Paleomagnetic and geochronologic constraints on the geodynamic evolution of the Central Dinarides. *Tectonophysics*, 530, 286–298.
- Dean, S., Morgan, J., & Fournier, T. (2013). Geometries of frontal fold and thrust belts: Insights from discrete element simulations. *Journal of Structural Geology*, 53, 43–53.
- Dragičević, I., Benić, J., & Blašković, I. (1985). Novi stratigrafski podaci o paleogenskim klastitima Studenih Vrila-Zapadna Hercegovina. *Geološki Vjesnik*, 38, 31–34.
- Dragičević, I., Blašković, I., Tišljar, J., & Benić, J. (1992). Stratigraphy of Paleogene Strata within the Mesihovina-Rakitno Area (Western Herzegovina). *Geologia Croatica*, 45(1), 25–52.
- Egan, S., Buddin, T., Kane, S., & Williams, G. (1997). Three-dimensional modelling and visualisation in structural geology: new techniques for the restoration and balancing of volumes. In Proceedings of the 1996 geoscience information group conference on geological visualisation. Electronic Geology Special Volume (pp. 67–82).
- Erdős, Z., Huismans, R. S., & van der Beek, P. (2015). First-order control of syntectonic sedimentation on crustal-scale structure of mountain belts. *Journal of Geophysical Research: Solid Earth*, 120(7), 5362–5377.
- Erdős, Z., Huismans, R. S., van der Beek, P., & Thieulot, C. (2014). Extensional inheritance and surface processes as controlling factors of mountain belt structure. *Journal of Geophysical Research: Solid Earth*, 119(12), 9042–9061.
- Erickson, S. G. (1995). Mechanics of triangle zones and passive-roof duplexes: Implications of finite-element models. *Tectonophysics*, 245(1–2), 1–11.
- Fillon, C., Huismans, R. S., & van der Beek, P. (2013). Syntectonic sedimentation effects on the growth of fold-and-thrust belts. *Geology*, 41(1), 83–86.
- Fio, K., et al. (2010). Stable isotope and trace element stratigraphy across the Permian-Triassic transition: A redefinition of the boundary in the Velebit Mountain, Croatia. *Chemical Geology*, 278(1–2), 38–57.
- Gibbs, A. (1983). Balanced cross-section construction from seismic sections in areas of extensional tectonics. *Journal of Structural Geology*, 5(2), 153–160.
- Gobo, K., Mrinjek, E., & Ćosović, V. (2020). Mass-transport deposits and the onset of wedge-top basin development: An example from the Dinaric Foreland Basin, Croatia. *Journal of Sedimentary Research*, 90(11), 1527–1548.
- Granado, P., & Ruh, J. B. (2019). Numerical modelling of inversion tectonics in fold-and-thrust belts. *Tectonophysics*, 763, 14–29.
- Grandić, S. (1974). Neke naftnogeološke karakteristike naslaga Vanj skih Dinarida [Some regional petroleum geological characteristics of the External Dinarides deposits]. *Nafta*, 25(3), 111–120. in Croatian.
- Graveleau, F., Malavielle, J., & Dominguez, S. (2012). Experimental modelling of orogenic wedges: A review. *Tectonophysics*, 538, 1–66.
- Grimani, I., Šikić, K., & Šimunić, A. (1972). *Osnovna geološka karta SFRJ 1:100,000, list Knin L33-141 (Basic geological map of SFRJ 1:100,000, Knin sheet)*. Institut za geološka istraživanja Zagreb, Savezni geološki zavod.
- Guimerà, J., Alonso, Á., & Mas, J. R. (1995). Inversion of an extensional-ramp basin by a newly formed thrust: The Cameros basin (N. Spain). *Geological Society, London, Special Publications*, 88(1), 433–453.
- Handy, M. R., et al. (2019). Coupled crust-mantle response to slab tearing, bending, and rollback along the Dinaride-Hellenide orogen. *Tectonics*, 38(8), 2803–2828.
- Hayward, A., & Graham, R. (1989). Some geometrical characteristics of inversion. *Geological Society, London, Special Publications*, 44(1), 17–39.
- Herak, D., et al. (2017). Historical seismicity of the Rijeka region (northwest external Dinarides, Croatia)—Part I: Earthquakes of 1750, 1838, and



- 1904 in the Bakar epicentral area. *Seismological Research Letters*, 88(3), 904–915.
- Herak, M., et al. (2011). Republika Hrvatska, Karta potresnih područja [Republic of Croatia, Seismic Hazard Maps]. University of Zagreb, Faculty of Science, Department of Geophysics. Retrieved July 9, 2022, from <http://seizkarta.gfz.hr/hazmap/karta.php> (in Croatian)
- Herak, M., et al. (2018). Historical seismicity of the Rijeka Region (Northwest External Dinarides, Croatia)—Part II: The Klana earthquakes of 1870. *Seismological Research Letters*, 89(4), 1524–1536.
- Herak, M., & Herak, D. (2021). Properties of the Zagreb 22 March 2020 earthquake sequence—Analyses of the full year of aftershock recording. *Geofizika*, 38, 93–116.
- Herak, M., Herak, D., & Markušić, S. (1996). Revision of the earthquake catalogue and seismicity of Croatia, 1908–1992. *Terra Nova*, 8(1), 86–94.
- Hombert, C., Bergerat, F., Philippe, Y., Lacombe, O., & Angelier, J. (2002). Structural inheritance and Cenozoic stress fields in the Jura fold-and-thrust belt (France). *Tectonophysics*, 357(1–4), 137–158.
- Horváth, F., et al. (2015). Evolution of the Pannonian basin and its geothermal resources. *Geothermics*, 53, 328–352.
- Ivanović, A., et al. (1973). *Osnovna geološka karta SFRJ 1:100,000, list Obrovac L 33-140 (Basic geological map of SFRY 1:100,000 Obrovac sheet)*. Institut za geološka istraživanja Zagreb, Savezni geološki zavod.
- Jamison, W. R. (1996). Mechanical models of triangle zone evolution. *Bulletin of Canadian Petroleum Geology*, 44(2), 180–194.
- Korolija, B., Živaljević, T., & Šimunić, A. (1979). *Osnovna geološka karta SFRJ 1:100,000, list Slunj L33-104 (Basic Geological Map of SFRY 1:100,000, Slunj Sheet)*. Institut za geološka istraživanja Zagreb, Savezni geološki zavod.
- Krnjak, H. (2019). *Structural-geological model of the Plitvice Lakes National Park area* (pp. 1–49). University of Zagreb.
- Kulušić, A., & Borojević Šostarić, S. (2014). Dinaride evaporite mélange: Diagenesis of the Kosovo polje evaporites. *Geologia Croatica*, 67(1), 59–74.
- Lake, S. D., & Karner, G. D. (1987). The structure and evolution of the Wessex Basin, southern England: An example of inversion tectonics. *Tectonophysics*, 137(1–4), 347–378.
- Laubach, S. E., Olson, J. E., & Gross, M. R. (2009). Mechanical and fracture stratigraphy. *AAPG Bulletin*, 93(11), 1413–1426.
- Lawrence, S., Tari-Kovačić, V., & Gjukić, B. (1995). Geological evolution model of the Dinarides. *Nafta*, 46(2), 103–113.
- Majcen, Z., Korolija, B., Sokač, B., & Nikler, L. (1970). *Osnovna geološka karta SFRJ 1:100,000, list Zadar L33-139 (Basic geological map of SFRY 1:100,000, Zadar sheet)*. Institut za geološka istraživanja Zagreb, Savezni geološki zavod.
- Malz, A., Madritsch, H., Meier, B., & Kley, J. (2016). An unusual triangle zone in the external northern Alpine foreland (Switzerland): Structural inheritance, kinematics and implications for the development of the adjacent Jura fold-and-thrust belt. *Tectonophysics*, 670, 127–143.
- Mamužić, P. (1971). *Osnovna geološka karta SFRJ 1:100,000, list Šibenik K33-8 (Basic geological map of SFRY 1:100,000, Šibenik sheet)*. Institut za geološka istraživanja Zagreb, Savezni geološki zavod.
- Mamužić, P., Korolija, B., et al. (1970a). *Osnovna geološka karta SFRJ 1:100,000, list Molat L33-138 (Basic geological map of SFRY 1:100,000, Molat sheet)*. Institut za geološka istraživanja Zagreb, Savezni geološki zavod.
- Mamužić, P., Milan, A., Korolija, B., Borović, I., & Majcen, Z. (1969). *Osnovna geološka karta SFRJ 1:100,000, list Rab L33-114 (Basic geological map of SFRY 1:100,000, Rab sheet)*. Institut za geološka istraživanja Zagreb, Savezni geološki zavod.
- Mamužić, P., & Nedela-Devide, D. (1968). *Osnovna geološka karta SFRJ 1:100,000, list Biograd K33-7 (Basic geological map of SFRY 1:100,000, Biograd sheet)*. Institut za geološka istraživanja Zagreb, Savezni geološki zavod.
- Mamužić, P., Sokač, B., & Velić, J. (1970b). *Osnovna geološka karta SFRJ 1:100,000, list Silba L33-126 (Basic geological map of SFRY 1:100,000, Silba sheet)*. Institut za geološka istraživanja Zagreb, Savezni geološki zavod.
- McQuillan, H. (1973). Small-scale fracture density in Asmari Formation of southwest Iran and its relation to bed thickness and structural setting. *AAPG Bulletin*, 57(12), 2367–2385.
- Mohn, G., Manatschal, G., Beltrando, M., & Hupert, I. (2014). The role of rift-inherited hyper-extension in Alpine-type orogens. *Terra Nova*, 26(5), 347–353.
- Mojičević, N., Maksimčev, S., & Vrhovčić, J. (1977). *Osnovna geološka karta SFRJ 1:100,000, list Bosanska Krupa L33-117 (Basic geological map of SFRJ 1:100,000, Bosanska Krupa sheet)*. Institut za geološka istraživanja Zagreb, Savezni geološki zavod.
- Molinari, I., et al. (2016). Swiss-AlpArray temporary broadband seismic stations deployment and noise characterization. *Advances in Geosciences*, 43, 15–29.
- Mrinjek, E., Nemec, W., Pecinger, V., Mikša, G., Vlahović, I., Čosović, V., Velić, I., Bergant, S., & Matičec, D. (2012). The Eocene-Oligocene Promina Beds of the Dinaric Foreland Basin in Northern Dalmatia. *Journal of Alpine Geology*, 55, 409–451.
- Mugnier, J., et al. (1997). Thrust geometry controlled by erosion and sedimentation: A view from analogue models. *Geology*, 25(5), 427–430.
- Mulugeta, G., & Koyi, H. (1992). Episodic accretion and strain partitioning in a model sand wedge. *Tectonophysics*, 202(2–4), 319–333.
- Narr, W. (1991). Fracture density in the deep subsurface: Techniques with application to Point Arguello oil field. *AAPG Bulletin*, 75(8), 1300–1323.
- Palenik, D., et al. (2019). Geological and structural setting of the Vinodol Valley (NW Adriatic, Croatia): Insights into its tectonic evolution based on structural investigations. *Geologia Croatica*, 72(3), 179–193.
- Pamić, J. J. (1984). Triassic magmatism of the Dinarides in Yugoslavia. *Tectonophysics*, 109(3–4), 273–307.
- Pamić, J., Tomljenović, B., & Balen, D. (2002). Geodynamic and petrogenetic evolution of Alpine ophiolites from the central and NW Dinarides: An overview. *Lithos*, 65(1–2), 113–142.
- Petersen, G. M., et al. (2021). Regional centroid moment tensor inversion of small to moderate earthquakes in the Alps using the dense AlpArray seismic network: Challenges and seismotectonic insights. *Solid Earth*, 12(6), 1233–1257.
- Picotti, V., & Cobianchi, M. (2017). Jurassic stratigraphy of the Belluno Basin and Friuli Platform: A perspective on far-field compression in the Adriatic passive margin. *Swiss Journal of Geosciences*, 110(3), 833–850.
- Polšak, A., Juriša, M., Šparica, M., & Šimunić, A. (1976). *Osnovna geološka karta SFRJ 1:100,000, list Bihać L33-116 (Basic geological map of SFRY 1:100,000, Bihać sheet)*. Institut za geološka istraživanja Zagreb, Savezni geološki zavod.
- Prtoljan, B., Jamicic, D., Tešovic, B. C., Kratkovic, I., & Markulin, Ž. (2007). The influence of Late Cretaceous synsedimentary deformation on the Cenozoic structuration of the middle Adriatic, Croatia. *Geodinamica Acta*, 20(5), 287–300.
- Ravaglia, A., Turrini, C., & Seno, S. (2004). Mechanical stratigraphy as a factor controlling the development of a sandbox transfer zone: A three-dimensional analysis. *Journal of Structural Geology*, 26(12), 2269–2283.
- Rich, J. L. (1934). Mechanics of low-angle overthrust faulting as illustrated by Cumberland thrust block, Virginia, Kentucky, and Tennessee. *AAPG Bulletin*, 18(12), 1584–1596.
- Robertson, A., Karamata, S., & Šarić, K. (2009). Overview of ophiolites and related units in the Late Palaeozoic–Early Cenozoic magmatic and tectonic development of Tethys in the northern part of the Balkan region. *Lithos*, 108(1–4), 1–36.
- Šćavničar, B., Šćavničar, S., & Šušnjara, A. (1984). The volcanic-sedimentary Middle Triassic in the Suvaja brook area (Mt. Svilaja, Outer Dinarides). *Acta Geologica*, 14(2), 35–82.
- Schmid, S. M., et al. (2020). Tectonic units of the Alpine collision zone between Eastern Alps and Western Turkey. *Gondwana Research*, 78, 308–374.
- Schmitz, B., et al. (2020). Ongoing shortening in the Dinarides fold-and-thrust belt: A new structural model of the 1979 (Mw 7.1) Montenegro earthquake epicentral region. *Journal of Structural Geology*, 141, 104192.
- Scisciani, V. (2009). Styles of positive inversion tectonics in the Central Apennines and in the Adriatic foreland: Implications for the evolution of the Apennine chain (Italy). *Journal of Structural Geology*, 31(11), 1276–1294.
- Scisciani, V., & Calamita, F. (2009). Active intraplate deformation within Adria: Examples from the Adriatic region. *Tectonophysics*, 476(1–2), 57–72.
- Scisciani, V., Tavarnelli, E., & Calamita, F. (2002). The interaction of extensional and contractional deformations in the outer zones of the Central Apennines, Italy. *Journal of Structural Geology*, 24(10), 1647–1658.
- Šiftar, D. (1982). Izotopni sustav sumpora i starost evaporita s primjerima iz područja Dinarida u južnoj Hrvatskoj. *Nafta*, 33(4), 177–183.
- Šiftar, D. (1986). Starost evaporita u području Sinj–gornji tok Une. *Geološki Vjesnik Zagreb*, 39, 55–60.
- Smirčić, D., et al. (2018). Stratigraphic definition and correlation of Middle Triassic volcanoclastic facies in the External Dinarides: Croatia and Bosnia and Herzegovina. *Journal of Earth Science*, 29(4), 864–878.

- Smirčić, D., Aljinović, D., Barudžija, U., & Kolar-Jurkovšek, T. (2020). Middle Triassic syntectonic sedimentation and volcanic influence in the central part of the External Dinarides, Croatia (Velebit Mts.). *Geological Quarterly*, 64(1), 220–239. <https://doi.org/10.7306/gq.1528>
- Sokač, B., Nikler, L., Velić, J., & Mamučić, P. (1974). *Osnovna geološka karta SFRJ 1:100,000, list Gospić K33-127 (Basic geological map of SFRY 1:100,000, Gospić sheet)*. Beograd: Institut za geološka istraživanja Zagreb, Savezni geološki zavod.
- Šrodoň, J., et al. (2018). Thermal history of the central part of the Karst Dinarides, Croatia: Combined application of clay mineralogy and low-T thermochronology. *Tectonophysics*, 744, 155–176.
- Suppe, J. (1983). Geometry and kinematics of fault-bend folding. *American Journal of Science*, 283(7), 684–721.
- Suppe, J. (1985). *Principles of structural geology*. Prentice-Hall.
- Suppe, J., & Medwedeff, D. A. (1990). Geometry and kinematics of fault-propagation folding. *Eclogae Geologicae Helvetiae*, 83(3), 409–454.
- Šušnjara, M., et al. (1973). *Osnovna geološka karta SFRJ 1:100,000, list Udbina L33-128 (Basic geological map of SFRY 1:100,000, Udbina sheet)*. Institut za geološka istraživanja Zagreb, Savezni geološki zavod.
- Šušnjara, M., & Bukovac, J. (1978). *Osnovna geološka karta SFRJ 1:100,000, list Drvar L33-129 (Basic geological map of SFRY 1:100,000, Drvar sheet)*. Institut za geološka istraživanja Zagreb, Savezni geološki zavod.
- Šušnjara, A., Sokač, K., Jelen, B., & Gabrić, A. (1992). Upper Permian evaporites and associated rocks of Dalmatia and borderline area of Lika and Bosnia. *Geologia Croatica*, 45(1), 95–114.
- Tavarnelli, E. (1996). Tethyan heritage in the development of the Neogene Umbria-Marche fold-and-thrust belt, Italy: A 3D approach. *Terra Nova*, 8(5), 470–478.
- Tavarnelli, E., et al. (2004). Implications of fault reactivation and structural inheritance in the Cenozoic tectonic evolution of Italy. *The Geology of Italy, Special*, 1, 209–222.
- Tešović, B. C., Martinuš, M., Golec, I., & Vlahović, I. (2020). Lithostratigraphy and biostratigraphy of the uppermost Cretaceous to lowermost Palaeogene shallow-marine succession: Top of the Adriatic Carbonate Platform at the Likva Cove section (island of Brač, Croatia). *Cretaceous Research*, 114, 104507.
- Tišljar, J. (1992). Origin and depositional environments of the evaporite and carbonate complex (Upper Permian) from the central part of the Dinarides (Southern Croatia and Western Bosnia). *Geologia Croatica*, 45(1), 115–126.
- Tišljar, J., Vlahović, I., Velić, I., Matičec, D., & Robson, J. (1998). Carbonate facies evolution from the Late Albian to Middle Cenomanian in southern Istria (Croatia): Influence of syndimentary tectonics and extensive organic carbonate production. *Facies*, 38(1), 137–151.
- Tončić-Gregl, R., & Prpić, N. (1971). Lithological, petrophysical, biostratigraphical and chronostratigraphical data from the exploration boreholes Ravni Kotari-3, Dugi Otok-1 and Premuda-1. *Nafta*, 22(4–5), 472–482.
- Turrini, C., Ravaglia, A., & Perotti, C. R. (2001). Compressional structures in a multilayered mechanical stratigraphy: Insights from sandbox modeling with three-dimensional variations in basal geometry and friction. *Geological Society of America Memoirs*, 193, 153–178.
- Ustaszewski, K., et al. (2009). Late Cretaceous intra-oceanic magmatism in the internal Dinarides (northern Bosnia and Herzegovina): Implications for the collision of the Adriatic and European plates. *Lithos*, 108(1–4), 106–125.
- Ustaszewski, K., Herak, M., Tomljenović, B., Herak, D., & Matej, S. (2014). Neotectonics of the Dinarides-Pannonian Basin transition and possible earthquake sources in the Banja Luka epicentral area. *Journal of Geodynamics*, 82, 52–68.
- Ustaszewski, K., Kounov, A., Schmid, S. M., Schaltegger, U., Krenn, E., Frank, W., & Fügenschuh, B. (2010). Evolution of the Adria-Europe plate boundary in the northern Dinarides: From continent-continent collision to back-arc extension. *Tectonics*, 29(6). <https://doi.org/10.1029/2010TC002668>.
- Ustaszewski, K., Schumacher, M. E., Schmid, S. M., & Nieuwland, D. (2005). Fault reactivation in brittle-viscous wrench systems—dynamically scaled analogue models and application to the Rhine-Bresse transfer zone. *Quaternary Science Reviews*, 24(3–4), 363–380.
- van Unen, M., et al. (2019). Transfer of deformation during indentation: Inferences from the post-middle Miocene evolution of the Dinarides. *Global and Planetary Change*, 182, 103027.
- Velić, I., Bahun, S., Sokač, B., & Galović, I. (1974). *Osnovna geološka karta SFRJ 1:100,000, list Otočac L33-115 (Basic geological map of SFRY 1:100,000, Otočac sheet)*. Institut za geološka istraživanja Zagreb, Savezni geološki zavod.
- Velić, I., Vlahović, I., & Matičec, D. (2002). Depositional sequences and Palaeogeography of the Adriatic Carbonate Platform. *Memorie della Società Geologica Italiana*, 57(1), 141–151.
- Vergés, J., Fernández, M., & Martínez, A. (2002). The Pyrenean orogen: Pre-, syn-, and post-collisional evolution. *Journal of the Virtual Explorer*, 8, 55–74.
- Verrall, P. (1981). Structural interpretation with applications to North Sea problems. Course notes No. 3. Joint Association for Petroleum Exploration Courses (UK).
- Vitzthum, M. A., Gawlick, H.-J., Sachsenhofer, R. F., & Neumeister, S. (2022). Changing depositional environments in the semi-restricted Late Jurassic Lemeš Basin (Outer Dinarides; Croatia). *Facies*, 68(1), 1–35.
- Vlahović, I., et al. (2012). Marine to continental depositional systems of Outer Dinarides foreland and intra-montane basins (Eocene-Miocene, Croatia and Bosnia and Herzegovina). *Journal of Alpine Geology*, 54, 405–470.
- Vlahović, I., Tišljara, J., Velić, I., & Matičec, D. (2005). Evolution of the Adriatic Carbonate Platform: Palaeogeography, main events and depositional dynamics. *Palaeogeography, Palaeoclimatology, Palaeoecology*, 220(3–4), 333–360.
- von Hagke, C., & Malz, A. (2018). Triangle zones—Geometry, kinematics, mechanics, and the need for appreciation of uncertainties. *Earth-Science Reviews*, 177, 24–42.
- Wilkins, S. J., & Gross, M. R. (2002). Normal fault growth in layered rocks at Split Mountain, Utah: Influence of mechanical stratigraphy on dip linkage, fault restriction and fault scaling. *Journal of Structural Geology*, 24(9), 1413–1429.
- Williams, G., Powell, C., & Cooper, M. (1989). Geometry and kinematics of inversion tectonics. *Geological Society, London, Special Publications*, 44(1), 3–15.
- Withjack, M. O., & Peterson, E. T. (1993). Prediction of normal-fault geometries—A sensitivity analysis. *AAPG Bulletin*, 77(11), 1860–1873.
- Žibret, L., & Vrabec, M. (2016). Paleostress and kinematic evolution of the orogen-parallel NW-SE striking faults in the NW External Dinarides of Slovenia unraveled by mesoscale fault-slip data analysis. *Geologia Croatica*, 69(3), 295–305.
- Zupanić, J., & Babić, L. (2011). Sedimentary evolution of an inner foreland basin margin: Paleogene Promina Beds of the type area, Mt. Promina (Dinarides, Croatia). *Geologia Croatica*, 64, 101–119.
- Zwaan, F., et al. (2022). Analogue modelling of basin inversion: A review and future perspectives. *Solid Earth Discussions*, 13, 1–84.

## Publisher's Note

Springer Nature remains neutral with regard to jurisdictional claims in published maps and institutional affiliations.

**Submit your manuscript to a SpringerOpen<sup>®</sup> journal and benefit from:**

- Convenient online submission
- Rigorous peer review
- Open access: articles freely available online
- High visibility within the field
- Retaining the copyright to your article

Submit your next manuscript at ► [springeropen.com](https://www.springeropen.com)